THERMAL CYCLING EFFECTS ON THE NANOPARTICLE DISTRIBUTION AND SPECIFIC HEAT OF A CARBONATE EUTECTIC WITH ALUMINA NANOPARTICLES

A Thesis

by

SANDHYA SHANKAR

Submitted to the Office of Graduate Studies of
Texas A&M University
in partial fulfillment of the requirements for the degree of

MASTER OF SCIENCE

May 2011

Major Subject: Mechanical Engineering

THERMAL CYCLING EFFECTS ON THE NANOPARTICLE DISTRIBUTION AND SPECIFIC HEAT OF A CARBONATE EUTECTIC WITH ALUMINA NANOPARTICLES

A Thesis

by

SANDHYA SHANKAR

Submitted to the Office of Graduate Studies of
Texas A&M University
in partial fulfillment of the requirements for the degree of

MASTER OF SCIENCE

Approved by:

Co-Chairs of Committee,	Sai Lau
	Thomas Lalk
Committee Member	Michael Schuller
Head of Department,	Dennis O'Neal

May 2011

Major Subject: Mechanical Engineering

ABSTRACT

Thermal Cycling Effects on the Nanoparticle Distribution and Specific Heat of a Carbonate Eutectic with Alumina Nanoparticles. (May 2011)

Sandhya Shankar, B.E.,Anna University, India

Chair of Advisory Committee: Dr. Sai Lau
Dr. Thomas Lalk

The objective of this research was to measure the effect of thermal cycling on the nanoparticle distribution and specific heat of a nanocomposite material consisting of a eutectic of lithium carbonate and potassium carbonate and 1% by mass alumina nanoparticles. The material was subjected to thermal cycling in a stainless steel tube using a temperature controlled furnace. After thermal cycling, the stainless steel tube was sectioned into three equal parts – top, middle and bottom. Composite material samples were taken from the central region and near the wall region of each section.

The specific heat of this material in the temperature range of 290°C-397°C was measured using the Modulated Differential Scanning Calorimeter (MDSC) method. The concentration of alumina nanoparticles in this material was measured using neutron activation analysis. The average specific heat of the uncycled material was found to be 1.37 J/g°C.The average specific heat of the thermally cycled material was between 1.7-2.1 J/g°C. It was found that the concentration of the nanoparticle varied along the height of the sample tube. The nanoparticles tended to settle towards the bottom of the tube with thermal cycling. There was also migration of nanoparticles towards the wall of the sample tube with thermal cycling. Despite these gross

movements of nanoparticles, there was no significant change in the specific heat of the nanocomposite due to thermal cycling.

ACKNOWLEDGEMENTS

I want to thank Dr.Schuller and other committee members for their guidance and support in this work. I want to thank my colleagues, Wan Zhong and Qian Shaong, for their assistance in this work. I also want to thank Dr.Debjyoti Banerjee for providing the nanomaterials required for this work. Finally, I would like to thank my parents and sisters.

NOMENCLATURE

C	Degrees Celsius
C_p	Specific Heat Capacity
cP	centiPoise
CSP	Concentrating Solar Power
d	Diameter
DOE	Department of Energy
DSC	Differential Scanning Calorimetry
g	Gram
hr	Hour
HTF	Heat Transfer Fluid
J	Joule
K	Kelvin
kg	Kilogram
m	Meter
MDSC	Modulated Differential Scanning Calorimetry
mg	Milligram
mL	Milliliter

NAA	Neutron Activation Analysis
nf	Nanofluid
PCM	Phase Change Material
PV	Photovoltaic
p	Particle
s	Second
SWCNT	Single Walled Carbon Nanotubes
TA	Thermal Analysis
TES	Thermal Energy Storage
ΔT	Change in temperature (T_H-T_L)

TABLE OF CONTENTS

Page

Page

LIST OF TABLES

Page

Page

LIST OF FIGURES

Page

Page

1. INTRODUCTION

1.1 Background

We have been dependent on fossil fuels to meet all of our requirements for energy. The gap between the demand and supply of the fossil fuels is widening compelling us to shift to cleaner and renewable sources of energy. Solar energy is one of the main forms of renewable energy available abundantly. Solar energy is collected by plants and stored in the form of chemical energy. Solar energy can be converted to electricity in two ways. Photovoltaic (PV) cells convert light energy to electric energy. An array of PV cells spread across a large area of land can be used to generate electricity on a large scale. A second method of exploiting solar energy is concentrating solar power plants (CSPs).

Concentrating solar power plants use solar energy to produce thermal energy, which is then used for electricity generation. The solar radiation is concentrated into a heat transfer fluid, which is then used to produce steam for running turbines. A major hurdle of CSPs is the unavailability of solar energy either during night time or during winter which makes them less dependable than fossil fuels as a source of energy. This lack of dependability marginalizes CSP. The integration of thermal energy storage systems (TESs) can combat this problem. The concept of energy storage and TES systems is discussed in the next few sections.

This thesis follows the style of Journal of Solar Energy Engineering.

1.2 Energy storage

Energy storage is the process of storing a form of energy in a storage medium, which can be drawn upon whenever required to perform some useful operation. Thermal energy storage is the method of storing thermal energy as either sensible or latent heat in an energy storage device, from which the energy can then be extracted at a later time to do useful work. TESs are being incorporated into systems for waste heat recovery, solar energy utilization, building energy management, and electronic device energy management.

The most compelling advantage of a TES system in power generation is load leveling. The peak demand for electricity is during the late afternoon and evening when the supply of solar energy is well below peak. A TES system bridges this gap between periods of supply and demand by temporarily storing the thermal energy from the collector fields and dispatching the energy to the generator whenever it is required. The integration of a TES reduces the need for any fossil fuel back-up system required to supplement periods of insufficient solar energy. This is illustrated in Figure 1 which shows the energy output of a power plant integrated with a TES system. The energy demand which is maximum during the night can be met with the energy stored during the day.

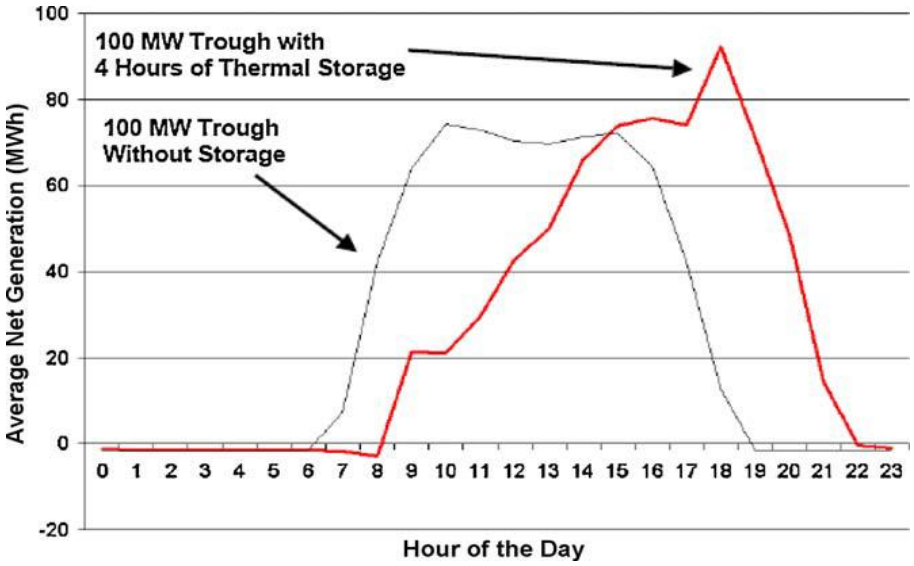

Figure 1 : Results of power dispatched with and without thermal storage system (1)

The desirable attributes of a TES system are: (2)

- Low cost
- High energy density of the storage material (storage capacity).
- Good heat transfer between heat transfer fluid (HTF) and the storage medium (efficiency).
- Mechanical and chemical stability of the storage material, which must support several charging/discharging cycles.
- Compatibility between HTF, the heat exchanger and/or the storage medium (safety).
- Complete reversibility of a number of charging/discharging cycles (lifetime).
- Low thermal losses.

- Ease of control.

All TES technology developed until now has achieved only few of the above attributes. However, there is not a single TES system that has exhibited all of them. A detailed discussion on the types of available storage media and the different methods for thermal storage is presented next. Knowledge of the types of the storage media and the available methods of storage is required to select the right TES system for our purpose.

1.3 Classification of thermal energy storage media

Thermal energy storage stores energy as sensible heat and/or latent heat. A sensible storage method uses the rise in temperature of the storage medium, which is usually a solid or a liquid. A latent storage method uses the enthalpy of a change of state to store thermal energy; such methods may also use sensible storage. Table 1 lists some commonly used thermal energy storage materials. Solid, liquid and phase change media that can be used as storage materials have been listed. The temperature range of operation will determine the maximum temperature of the storage system. The molten salts have very high temperature range allowing them to be used for high temperature storage systems.

Table 1 : Types of storage media and their cost (2)

Storage Medium	Temperature (°C)		Media Cost per kg (US $/kg)	Media cost per kWh (US $/kWh)
	Cold	Hot		
Solid Media				
Reinforced concrete	200	400	0.05	1.0
NaCl (Solid)	200	500	0.15	1.5
Sand rock mineral oil	200	300	0.15	4.2
Liquid Media				
Mineral Oil	200	300	0.30	4.2
Nitrate Salt	265	565	0.5	3.7
Carbonate Salt	450	850	2.4	11.0
Phase Change Media				
NaNO3	308		0.2	3.6
KNO3	333		0.3	4.1
Na2CO3	854		0.2	2.6
K2CO3	897		0.6	9.1

1.3.1 Sensible heat storage materials

The heat transfer to a sensible energy storage material increases its temperature. The energy stored is a product of the mass, the specific heat capacity and change in temperature of the material. Therefore, operating temperature, density, and the specific heat of the material determine the energy storage density of the system. The energy density of a storage material can be used to estimate the size of the storage system which in turn give the cost of storage. The energy density will increase with an increase in the specific heat of the material. Table 1 (above) shows some of the solid and liquid media used for energy storage and the energy density of each medium. Ultimately, the cost of each medium is an important factor when selecting a medium.

1.3.2 Latent heat storage material

In some materials, the addition of thermal energy induces a phase transformation, and that energy is stored as latent energy of the material. Such materials are called phase change materials (PCM). The phase change stores energy under isothermal conditions. Some PCM also use sensible heat storage to store energy.

1.3.3 Classification based on the concept of storage

Figure 2 shows the classification of TES systems based on the concept of storage. Storage systems can be classified as active or passive. In an active storage system, the storage material is circulated through the heat receivers and the heat exchangers where it is heated by the HTF. A passive storage system uses two or more media. The heat transfer fluid (HTF) circulates through the system, while the storage medium is stationary. The active storage can in turn be classified into direct and indirect storage systems. A detailed explanation of each type of storage system with examples has been given further.

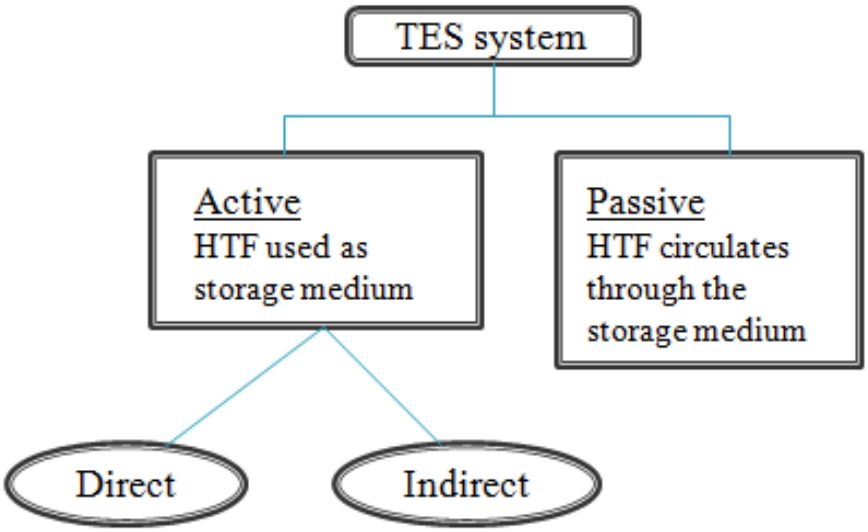

Figure 2 : Classification of TES systems based on the concept of storage

1.3.3.1 Active storage systems

An active storage system consists of a storage medium which acts as the HTF.The hot fluid coming from the collector fields is stored separately in a hot tank. The cold fluid coming from the generator systems is stored in another tank. Active storage systems can be further classified as direct and indirect.

In an active direct system, the HTF is also used as a storage material. When steam or molten salt is used for high temperature applications, it eliminates the heat exchangers from the system, which in turn reduces the cost of the system. A drawback of using molten salt is the danger of freezing of salt in the pipes, even at high temperatures, which requires an auxiliary heating system to ensure freeze protection of the salt.

A schematic of an active direct storage system is shown in Figure 3.The two-tank system is an active direct storage system where HTF circulated through the collectors is stored in a hot tank. The cold fluid coming out of the steam generator system is stored in a separate cold tank, and then is circulated through the collector field, where it is heated again.

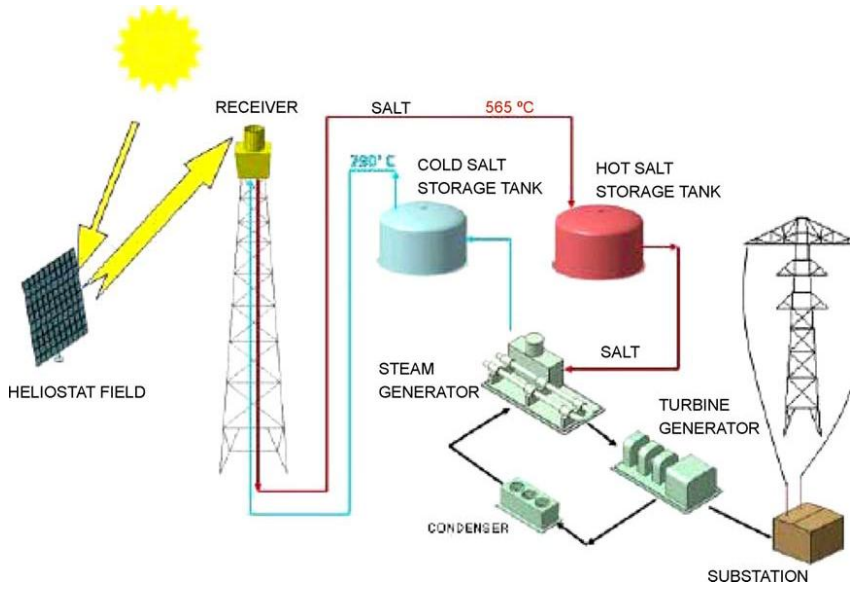

Figure 3: Schematic of an active direct storage system (Solar Tres Power Plant) (3)

The SEGS I plant included a direct two-tank storage system with a 3-hour full load energy capacity. In this plant, Caloria, a mineral oil, was used as the HTF and the storage material. After heating, the oil was stored in a hot tank at 307°C. After discharging its thermal energy in the power block, cold oil was stored in a cold tank at 240°C. The Caloria oil had a very high vaporpressure, and using it at high operating temperature required pressurized vessels which are expensive (4).

The Solar Two power plant uses a two tank storage system. It was designed to deliver thermal energy for three hours at the rated hot and cold salt temperatures of 565°C and 290°C.The total

storage capacity was 105 MWh. The storage media was molten salt consisting of a mixture of 60% sodium nitrate and 40% potassium nitrate. This mixture had a high density, low vapor pressure, and moderate specific heat, and was thermally stable up to 600°C (5).

The Solar Tres Power plant at Seville, Spain also uses Solar Two's two-tank direct method of storage using a nitrate mixture molten salt as the storage medium. The molten storage tank has a storage capacity of 600 MWh for a period of 15 hours (4).

An indirect two-tank system is similar to a two tank direct system which uses two tanks – one hot and another cold – to store the storage medium. But a HTF transfers heat through a heat exchanger. In a charging cycle, HTF at a high temperature from the collector fields circulates through a heat exchanger and heats the storage medium coming from the cold tank. The oil cools down and is recirculated to the collector field while the storage medium is heated and is stored in a hot tank. In a discharge cycle, heat from the storage medium is transferred through a heat exchanger to the HTF, which flows through the steam generator for power generation.

Thermocline type of storage is another active indirect method of storage where the hot and the cold fluids are stored in the same tank. The hot and cold fluids are separated by thermal stratification. The hot fluid passes through a heat exchanger which stores the heat in a thermal storage medium. The Solar One power plant incorporated a thermocline system of storage (6). The thermocline tank used rocks and sand as the filler material and oil as the HTF.The advantage of a thermocline system is the usage of a single tank, as opposed to a two-tank system. Using a low-cost filler material will lower the cost of the system. The disadvantages of a thermocline system are that it is difficult to separate the hot and cold HTF, that the high outlet temperature drives to an increase of losses in the solar field, that maintaining thermal stratification requires a controlled charging and discharging procedure and appropriate methods or devices to avoid

mixing, that the design of the storage system is complex, and that thermodynamically, it is an inefficient power plant (4).

1.3.3.2 Passive storage systems

A passive storage medium is a dual storage medium in which heat transfer fluid circulates through the storage medium. The storage medium, which is usually a solid (such as concrete or a PCM), does not circulate. Such a system uses a tube heat exchanger to transfer the heat from the HTF to the solid thermal storage material. A tube heat exchanger provides good contact and enables efficient heat exchange between the HTF and the solid storage medium. The thermo-physical properties of the solid sensible storage medium such as density, specific heat, vapor density, thermal conductivity, and thermal cycling stability, are important. The Solar de Almeria is one such passive storage system which uses sensible energy storage of a solid media for thermal storage.

A hybrid storage system proposed by the German DLR-ZSW uses a combination of latent heat and sensible heat storage. A prototype of the hybrid storage system in Stuttgart used synthetic oil as the HTF and three storage materials – sodium nitrate, concrete and a mixture of NaOH/NaCl.

Molten salts have become very popular as TES media due to their high operating temperatures, low vapor density and low cost. Among the many available salt systems, carbonates and nitrates are the two candidates of interest for this project. These two salt systems were chosen for their high operating temperature, low vapor density, low cost, and various others factors. In this particular thesis, the carbonate eutectic has been further researched, particularly with respect to effects of thermal cycling on the properties of the material. The term thermal cycling has been explained in detail in the theory section.

2. THEORY

This section outlines the theory of carbonates as an energy storage medium and on the improvement of the specific heat of the carbonate eutectic. (A eutectic is a mixture of several components, which melts sharply at a single temperature below the melting point of any individual component) .Thermal cycling testing of the material and its importance is discussed. Finally the Stokes model for calculating the settling time of the nanoparticles is discussed.

2.1 Carbonate as PCM for high temperature thermal energy storage

Materials used for thermal storage should have a high energy storage density. This reduces the size of the storage vessel and the related material cost, thus making the TES system economically sound. Among the various TES materials, alkali carbonates are a good candidate for thermal energy storage in high temperature applications. They have a high energy storage capacity, good thermal conductivity, low corrosiveness, moderate cost, and safe and simple handling procedures (7). The carbonate eutectic that was investigated is a eutectic of lithium carbonate and potassium carbonate. The phase diagram for the eutectic is shown in Figure 4. The eutectic is composed of 62% lithium carbonate and 38% potassium carbonate. The eutectic of this composition has a melting point of 488°C. The melting points of the pure components, lithium carbonate and potassium carbonate, are 723°C and 898°C respectively (8). Such a high melting point allows high temperature thermal energy storage and results in a high Rankine cycle efficiency of the power plants. One of the properties of phase change materials that make a considerable impact on thermal storage devices is the change in the volume of the material at phase transition. The volume of carbonate eutectic increases by 8.5% when it melts, which is not very high, and is well within the allowable range.

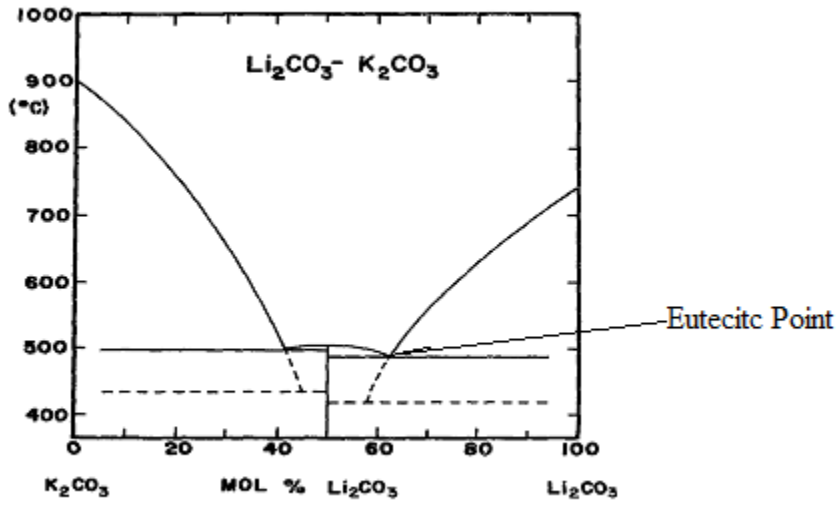

Figure 4 : Phase diagram of lithium carbonate and potassium carbonate (8)

Araki *et al* (9) used the following relationship to calculate the specific heat of carbonate eutectic in the solid phase with an uncertainty of ±3%:

$$Cp = 0.562 + 1.16 * 10^{-3} * T \text{ kJ.kg}^{-1}\text{.K at } 365 < T < 631K \quad [1]$$

The specific heat of the pure carbonate eutectic was measured in the lab. The results are discussed under the results and discussion section.

2.2 Effect of addition of nanoparticles on the specific heat

Materials created by introducing nanoparticles into a base material are called nanocomposites. The process of creating nanocomposites involves embedding nano- or molecular sized particles into organic polymers, ceramic materials, and/or metals. The intimate inclusion of the nanoparticles in the base material can completely change the properties of these base materials, and can drastically increase their electrical and thermal conductivity, as well as to their

mechanical strength(10). Molten salts are stable at high temperature (up to 600°C), non-toxic and cheap. However, their low specific heat, and therefore low energy storage density, increases the storage system cost and along with it the maintenance and operation costs. Therefore, improving the specific heat of the storage materials will increase the energy storage density of the system and reduce the overall system cost.

The effect of addition of nanoparticles in small concentrations have been observed and recorded. Some of them have been presented here. By studying these cases , it has been proposed that the addition of nanoparticles to molten salt will enhance the specific heat of the molten salts.

The addition of nanoparticles in small concentration to a liquid enhances the thermal conductivity of the liquid. This suspension of nanoparticles in a liquid is called a "nanofluid." Choi *et al* (11) demonstrated the enhancement of thermal conductivity of fluids with the addition of copper nanoparticles. Since then, several others have studied the change in thermal properties through the addition of nanoparticles and various theories to explain thermal transport in nanofluids have also been proposed.

The enhancement of specific heat with the addition of nanoparticles is a little-researched phenomenon. There has been some interest in the influence of nanoparticles on the specific heat of the base material. The enhancement of the specific heat of the liquids by the addition of nanoparticles has been observed by Zhou and Ni (12). They measured the specific heat of water-based alumina nanofluid with a differential scanning calorimeter. They observed the decrease of the specific heat of a nanofluid with the increase in volume fraction of nanoparticles. They found that a model based on the mixing theory of ideal gases failed to predict the specific heat of the nanofluid. Xuan and Roetzal's equation (13), shown below, which assumes that the nanoparticles

and the base material are in thermal equilibrium with each other, was in agreement with the specific heat of the nanofluid:

$$C_{p,nf} = \frac{\varphi(\rho C_p)_n + (1-\varphi)(\rho C_p)_f}{\varphi\rho_n + (1-\varphi)\rho_f} \qquad [2]$$

φ – volume fraction of nanoparticle

ρ – density

C_p – Specific heat

n – nanoparticle

f – fluid

nf - nanofluid

Vajjha and Das measured the specific heat of alumina, zinc oxide and silica nanofluids. A new correlation for the specific heat of the nanofluid was developed as a function of the particle volume concentration, temperature, and specific heat of both the particle and the base fluid. (14)

Shadab *et al* studied the enhancement of the latent heat of fusion of paraffin which was doped with carbon nanotubes (10). The change in latent heat was modeled using an approximation for the intermolecular attraction based on the Lennard-Jones potential. They concluded that the high molecular density of the SWCNT and its larger surface area were the reasons behind the greater intermolecular attraction in the wax/SWCNT composite, which resulted in its enhanced latent energy.

Phase I of the Department of Energy sponsored project studied and observed enhancement of the specific heat of molten salt (carbonate and nitrate) with the addition of nanoparticles in small concentration. The enhancement of specific heat of the "nanocomposites" in turn reduces the storage cost and thereby creates an overall reduction in cost for the TES system.

2.3 Thermal stability of the nanocomposites

For a material to be used as a phase change thermal energy storage material, it is essential that it exhibit the same thermal properties after repeated freeze-melt cycles. This ability to repeat the same thermal performance during charging and discharging over many cycles is termed the thermal stability, or thermal reliability, of the thermal energy storage material.

One of the attributes of a TES material is thermal reliability and long-term thermal cycling effects on the thermal properties material. The thermal properties and thermal reliability of thermal energy storage material must be verified by a thermal cycling life test to ensure the longevity of the TES system in which the material is used.

The economic feasibility of employing a thermal energy storage material in a system depends on the lifespan and cost of the storage materials used. Thermal cycling tests on phase change materials have been carried out with TES materials (15,16). The TES material is subjected to a certain number of thermal cycles. The thermal cycle used in this investigation is designed to emulate the charging and discharging cycle of the TES system. The thermal properties of the material are determined after a certain number of thermal cycles in order to measure the thermal stability of the thermal properties of the material after thermal cycling.

The results of the thermal cycling test have been used to determine whether the nanomaterial retains a similar thermal performance after thermal cycling and has good thermal stability, which will determine the suitability of the material for long-term usage in concentrating power plants.

One factor that affects the performance of the nanocomposite is the concentration of the nanoparticles in the material. The nanoparticles have to be dispersed uniformly throughout the material to maintain homogeneity of properties. The nanoparticles have a tendency to settle or agglomerate due to gravity, which disturbs the distribution of the nanoparticles within the material. During the thermal cycling the eutectic mixture is melted and the is maintained in this molten state for an hour during each cycle. The nanoparticles which are still in the solid phase will tend to settle. The extent of settling of the nanoparticles in the material with thermal cycling, and its change in the thermal properties caused due to the variation in concentration of nanoparticles as a result of the settling is determined. The concentration of nanoparticles in different sections of the sample material is measured and the extent of the settling of the nanoparticles is determined. In this experiment, the variation of concentration (and with it the specific heat) across the height of the test container has been measured.

To predict the extent of settling of nanoparticles, settling velocity based on Stokes' law is calculated. The settling velocity of the nanoparticle cluster is calculated in the following section.

2.4 Settling of nanoparticles – Stokes model for calculation of settling time

A thermal ratcheting test involves taking the material through multiple melt-freeze cycles. The time period for which the material is held at the melting point is determined by the time taken by the nanoparticles to settle in the base carbonate eutectic in the liquid state. This settling time is a function of the particle size, particle shape, wall effects, and density of the fluid medium. The

unhindered settling or the clustering of the particles in the suspension also influence the settling time.

The model used for calculation of the settling time assumes that the nanoparticles are perfect spheres and are distributed evenly within the fluid, which is assumed to be in an undisturbed state. The terminal settling velocity is estimated using the formula for the settling velocity of a particle in a creep flow.

The settling velocity of a single sphere in the liquid medium is given by:

$$w_o = \frac{d^2\ (\rho_P - \rho_F)}{18\mu} \qquad [3]$$

where

w_o – Settling velocity of the particle (ms^{-1})

g – Acceleration due to gravity (9.81 ms^{-2})

d – Diameter of the particle (m)

μ - dynamic viscosity of the fluid (base carbonate in the molten state)

= 9.813 cP (at T = 550°C) (8)

Density of eutectic ρ_F = 2.06 g/cm^3 (8)

Density of the nanoparticle ρP= 3.97 g/cm^3 (17)

Using the above formula, and assuming the diameter of an average cluster of nanoparticles to be between 30 nm (as isolated nanoparticles) and 5 microns, the settling velocity of the nanoparticles in the undisturbed fluid lies between $9.54*10^{-12}$ m/s and $2.65*10^{-7}$ m/s.

The settling time for a 50-micron particle in a 3-inch column of the molten salt is 0.79 hours. The settling time for a 30-nm particle is 2.21*10^6 hours.

The high viscosity of the fluid and the small difference in density between the particles and the medium gives rise to a low settling velocity and a long settling time.

The formula used to calculate the settling velocity does not account for the presence of other particles in the medium. It also assumes that the particles are spherical and the clusters formed are also spherical.

The largest clusters of nanoparticles, for the purpose of this investigation, have been assumed to be 20 microns. The percentage of nanoparticle clusters present in the nanomaterial will determine the concentration of nanoparticles settled at the bottom of the molten fluid column.

If the nanomaterial has no clusters, then the fluid can be held for long hours during the charging cycle. But as the cluster size increases, the settling time decreases, and with it the concentration of nanoparticles settling towards the bottom of the cylinder also increases.

Using this predicted value of settling time for a 20 micron cluster , the temperature profile for the thermal cycle will be designed in such a way that the nanomaterial is held in the molten state for at least one hour during each cycle. The time taken by a 20 micron nanoparticle cluster to settle towards the bottom of the sample tube is 16 hours. Allowing an additional 4 hours for any effect due to the wall, the sample will undergo 20 thermal cycles. After completion of 20 thermal

cycles the concentration of alumina in the top, middle and bottom section of the sample tube will be measured to determine the extent of settling of nanoparticles.

The material which has undergone 1 thermal cycle will serve as a useful reference point to determine the extent of settling. The material is allowed to undergo 40 and 60 thermal cycles in order to study the effect of prolonged thermal cycling on the material. The thermal cycling test and the temperature profile used for the thermal cycling is described in the next section.

2.5 Thermal cycling test

The temperature profile of the thermal cycling test is designed such that it emulates the thermal cycle taking place in an actual operating plant. Therefore the temperature profile is designed by looking at the charging and discharging time of an operating TES system. The charging and discharging time in a TES system depends on the rate at which the thermal gradient changes across the entire height of the storage tank. This is a property of both the material and the rate at which the storage material is pumped through the storage tank. Because of the height required for the gradient, taller tanks with smaller diameters are favored over shorter tank with larger diameters. The tallest tanks that can practically be fabricated have a bed height of 16 m. (6)

The aim through this thermal cycling test is to study the change in thermal properties of the TES material due to the dispersion of the nanoparticles. The thermal cycling test should therefore span for a sufficient time period that allows one to study the dispersion of nanoparticles.

While Brownian motion, diffusion, Van der Waals forces, and thermophoresis effects cause the agglomeration of nanoparticles, for the sake of simplicity only the agglomeration due to gravitational settling has been considered in this case.

Using a simple model based on Stokes law), the time for a 20-micron cluster of nanoparticles to settle in a test cylinder 3 inches high was calculated to be 16 hours. Using the same model, the settling time for 30 nm particles was calculated to be 2.21 *10^6 hours.

This shows that while well-dispersed nanoparticles are stable, clusters tend to settle quickly with time. Consider that the size of the nanoparticles/nanoclusters in the test sample ranges between 30 nm and 10 microns in size. Any cluster of size greater than 10 microns would settle faster than the 10-micron particles. The time taken for all the 10 micron clusters to settle through a distance of 3 inches in the test cylinder due to gravity is 20 hours.

The TES system contains the storage tank with the molten salt. A heat transfer fluid is used during charging and discharging to transfer heat to and from the molten salt. In a thermocline system, the temperature distribution varies along the vertical direction. The orientation of the heat exchanger tubes therefore determines the direction of the thermal gradient.

For a test cylinder 3 inches in height, it has been calculated that a 10 micron cluster would settle in 20 hours. Therefore, to test the model, the material has to be held in the liquid state for 20 hours, and the gradient in the nanoparticle concentration along the vertical column of the cylinder has to be measured. The melting point of the eutectic is 490°C and the material is held in the molten state at 550°C to allow the nanoparticles to settle. Typical TES systems operate between 300°C to 400°C.In this experiment thermal cycle in the temperature range of 300°C to 550°C is carried out. The temperature profile followed during each thermal cycle is described next.

A single thermal cycle is carried out between 300°C and 550°C. The material is heated from 300°C to 500°C in half an hour. The material is allowed to melt at 500°C for 1 hour. The

charging and discharging time is 1 hour each. This heating time is to ensure that the entire material in the cylinder is in the molten state. From 500°C the material is heated to 550°C and held in the liquid state for 1 hour. The material is then cooled back to the initial temperature of 300°C. This completes a single thermal cycle. The material inside the cylinder will be uniformly liquid at 550°C. Therefore the sample is in the liquid state for 1 hour during each thermal cycle. A single thermal cycle is 7 hours long.

The material is held in the liquid state for at least 20 hours in order to observe any settling of nanoparticles. The material is tested after 20, 40, and 60 cycles to determine its behavior after the estimated 20 hours of settling time. It is noted that a typical storage plant will have a discharging and charging time of 6-10 hours depending on the storage capacity of the plant. This time period depends on the storage density of the TES material used. In order to study the agglomeration of the nanoparticles and the changes in thermal properties in the material due to that agglomeration, the discharging and charging times have been scaled to the size of the test sample cylinder used for this experiment. The thermal profile is shown in Figure 5:

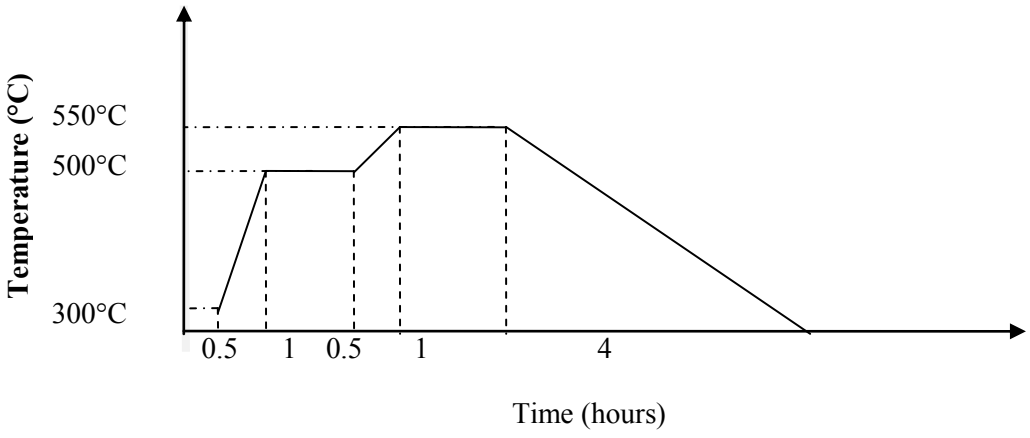

Figure 5 : Temperature profile followed by a single thermal cycle

This concludes this introduction to the concept of thermal storage, the enhancement of the specific heat of the material, thermal cycling and other topics related to this work. The next section explains in detail the procedures and instruments used to collect data for this thesis.

3. EXPERIMENTAL PROCEDURE

This section explains the experimental procedures involved in the preparation of the nanomaterial, the thermal cycling test, measurement of the specific heat of the nanomaterial, and the measurement of the concentration of the nanoparticles.

Nanocomposite material from carbonate eutectic with 1% concentration of alumina nanoparticles is prepared in the lab. The composite material is taken in stainless steel cylindrical tubing. This cylindrical tubing (sample container) is placed in a temperature-controlled programmable furnace where it undergoes thermal cycling. This "thermally cycled" material is then taken out of the furnace. The cylindrical tubing is sectioned into 3 equal parts – top, middle and bottom. . Material taken out of each of these sections is then subjected to tests using the Differential Scanning Calorimeter to measure its specific heat. Neutron activation analysis is used to determine the concentration of nanoparticles in the sample.

3.1 Material preparation

Nanomaterial is created by suspending the nanoparticles (alumina) and the base material (lithium carbonate/potassium carbonate eutectic) in an aqueous solution and then sonicating the solution to evenly disperse the nanoparticles in the salt. The water is evaporated by heating on a hot plate. A composite consisting of a lithium carbonate/potassium carbonate eutectic containing 1% alumina nanoparticles (by mass) is used.

The nanomaterial for this work is created in batches of 10 grams. To create the eutectic, 4.61 g of lithium carbonate and 5.29 g of potassium carbonate are taken in a jar, and 0.5 g of a 20% solution of aluminum oxide is added to the carbonates using a pipette. The contents are dissolved in distilled water. The solution is sonicated for 90 minutes. After sonication, the solution is heated on a hot plate at 300°C to 350°C without allowing the solution to boil. When all the water

is removed by evaporation, the nanomaterial that is left behind is collected by scrapping from the container. Material for this work is obtained by repeating the process six times to prepare 60 g of material. Since the carbonate is hygroscopic in nature, the nanomaterial is stored in a moisture free environment inside a glove box.

The specific heat and the concentration of nanoparticles of each batch of the nanomaterial are measured in order (see Results) to establish the uniformity of the starting material.

The mass of material used in this experiment is balanced between the cost of the material and total amount of material required to avoid any interference in settling behavior because of wall effects of the cylindrical container. The dimensions of the sample cylinder which contains the material for the thermal cycling tests cannot be too small, or else most of the material will adhere to the wall of the container. A large quantity of material, on the other hand, is more expensive, and more time is required to prepare the material.

3.2 Thermal cycling test

The nanomaterial is subjected to thermal cycling in a stainless steel sample container. The nanomaterial is held in 316 SS grade stainless steel cylinders of 3/8"' diameter and whose height is 3". The cylinder's dimensions should enable us to emulate actual plant operation in a laboratory setup. (In this case, the dimensions of the cylinder are also restricted because the nanomaterial is expensive and requires lengthy preparation. Therefore an optimum test sample size was determined arbitrarily for this test.) The sample holder is shown in Figure 6.

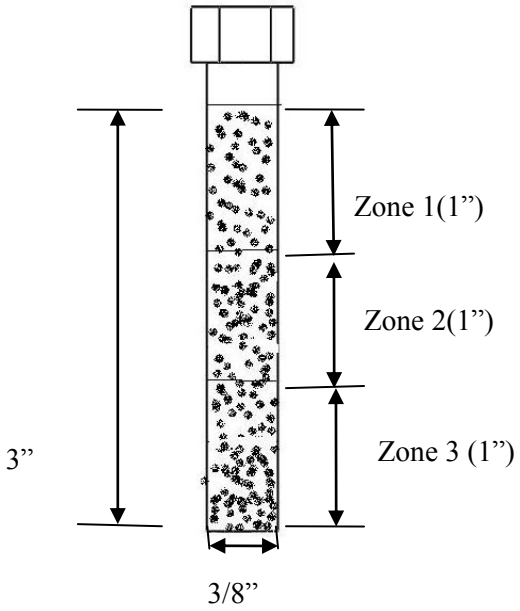

Figure 6 : Schematic representation of a sample holder with the nanomaterial and the different zones for study (All dimensions are in inches)

The cylinder was sealed with Swagelok compression fittings on one end and welded on the other end. There are 4 batches of sample material total that were subjected to thermal cycling. Each batch contained 3 sample cylinders. In total, 12 sample cylinders were thermally cycled. Each batch underwent a different number of thermal cycles and was therefore kept in the furnace for a different length of time. Table 2 shows the number of thermal cycles each batch of sample material underwent:

Table 2 : Number of thermal cycles undergone by each batch of thermally cycled material

Batch	Number of cycles
A	1
B	20
C	40
D	60

The thermal cycling was carried out in a Linderburg Blue 3 zone tube furnace with a UP 150 programmable temperature controller. The controller was programmed with the cycle following the temperature profile described in Figure 5.

3.3 Extraction of materials for analysis

The sample cylinders were taken out of the furnace after completion of the thermal cycles. The study of the gradient in the concentration of nanoparticles along the height of the sample container requires analyzing material from multiple sections of the specimen. In accordance with the preliminary nature of this study, thermo physical property will be characterized by taking material from 3 zones – top (zone 1), middle (zone 2), bottom (zone 3).

The sample cylinder is sectioned with a tube cutter to avoid any contamination of the material. The section is then allowed to soak in a dish of water .This makes the material soft so that it can be removed with minimal effort. The entire process is carried out in a glove box in a controlled argon atmosphere. The material removed from the sections is stored in glass vial. Any water present in the material is evaporated, and the material that was tested in the DSC is stored in a glove box with desiccants to keep the material moisture-free. The Figure 7 shows a schematic representation of the total number of samples used in this work.

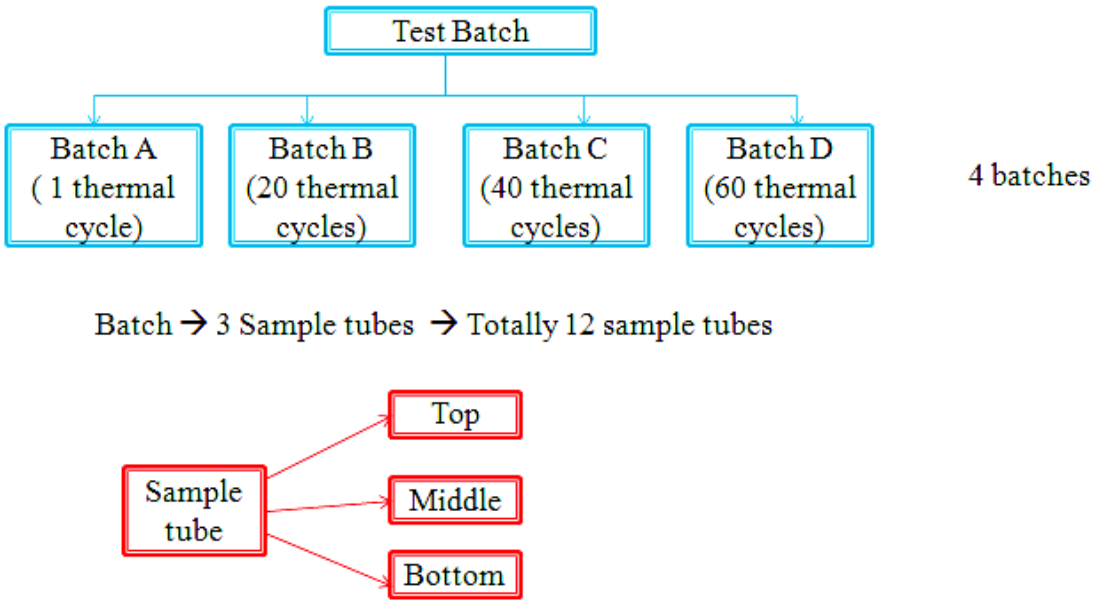

Figure 7 : Layout of the total number of samples in this thesis

3.4 Measurement of specific heat - modulated differential scanning calorimeter

The Modulated Differential Scanning Calorimeter (MDSC) is used to measure the specific heat of the material. The properties of the material are measured before and after the material are subjected to the thermal cycles. The modulated DSC differs from the ordinary DSC in the method of measurement: MDSC separates the total heat flow of DSC into two parts based on the heat flow that does and does not respond to a changing heating rate. MDSC applies a changing heating rate in addition to a fixed heating rate in order to measure the temperature change in response to the changing heating rate. In general, only heat capacity responds to the changing heating rate.

The specific heat of the sample at any point of time in the MDSC is given by the equation:

$$C_p = \frac{(\frac{dQ}{dt} - f(t,T))}{\frac{dT}{dt}} \qquad [4]$$

$\frac{dQ}{dt}$ - Differential heat flow rate (Watt)

Cp - Specific heat capacity (J/g°K)

$\frac{dT}{dt}$ - Ramp rate (°K/s)

$f(t,T)$ - Kinetic heat flow rate (Watt)

The first term on the right-hand side of equation [4] is a function of the heat flow rate, and the second term is a function of time and temperature. Kinetic events are a function of both time and temperature. Therefore kinetic events such as evaporation, decomposition, etc., shift to a higher temperature at higher heating rate. In an MDSC a sinusoidal modulation is overlaid on the conventional fixed heating ramp. By using a sinusoidal change in heating rate, an MDSC can separate the total heat flow signal into its heat capacity and kinetic components in a single experiment.

In an MDSC the actual heating rate depends on the following parameters (18):

- Underlying heat rate.
- Temperature amplitude of modulation.

Guidelines provided by TA Instruments were used to establish the experimental parameters. A heating rate lower than that used by a conventional DSC is preferred in order to allow sufficient

modulations during a thermal event. A heating rate of 4°C/min was used in this experiment. The larger the amplitude of modulation, the larger the heat flow rate response, since the instantaneous heating rate is directly related to the amplitude. Although larger amplitudes increase the sensitivities of signal for transition, too great amplitude may result in a situation where the material cannot follow the modulation. For this particular case, the amplitude was also selected so as to only heat the sample, not cool it. Amplitude of ±1°C was used, with a time period of 120 seconds.

Nitrogen was used as the purge gas for the cell. A sample size of 7-15 mg was used. The sample and the reference pan were closely matched in mass. The pans were crimped after being loaded with the sample. A microbalance was used to weigh the samples and the DSC pans.

A sapphire standard was used as the reference to establish the cell constant and determine the percentage error of the measured value in the temperature range of interest .The results of the sapphire check performed on the cell prior to obtaining results for sample runs have been shown in Figure 8. An average of 1.2 % of error over the temperature range of 290°C - 400°C was obtained.

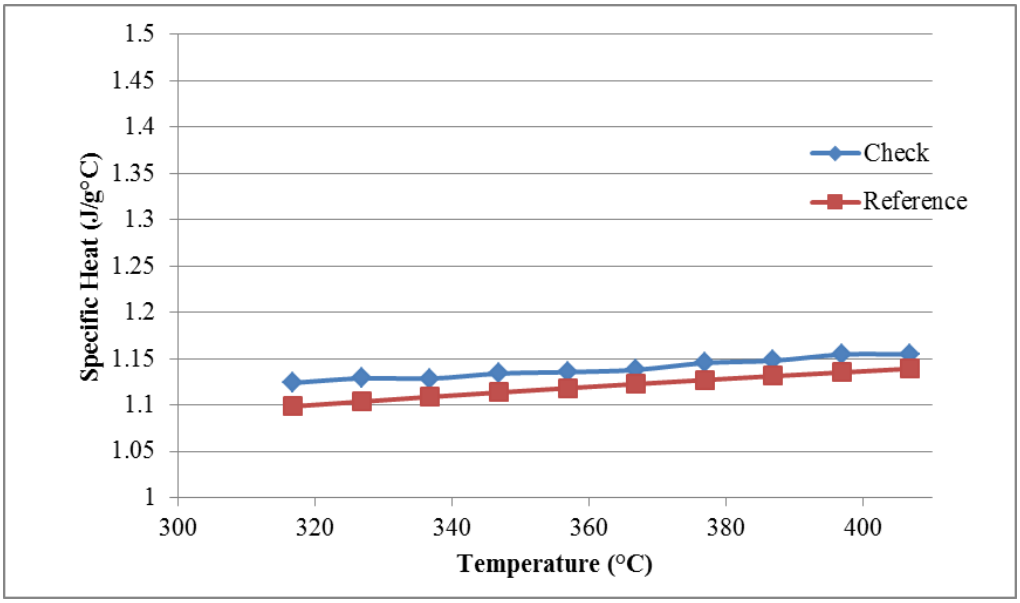

Figure 8 : Comparison between results of the sapphire check runs and the actual reference value

An important aspect of the MDSC is that the material must be able to follow the temperature profile imposed on it. The carbonate eutectic has a melting point of 490°C, and the reversible Cp of the material in the solid phase is of interest in this experiment. The temperature profile for this study starts with rapidly melting the material. The sample is then cooled down to 275°C and equilibrated at that temperature. It is then heated up to 410°C under modulated conditions with a time period of 120 seconds, a modulated temperature amplitude of ± 1°C, and a ramp rate of 4 °C/min. There are 3 cycles in each run. The modulation parameters are triggered for each cycle after the initial fast ramped melting of the sample. The modulation starts at 275°C and ends at 410°C, which marks the end of the cycle. The MDSC parameters are triggered for the temperature range where the reversible Cp of the sample will be recorded. The data obtained from the second and third cycles are taken into account for all calculations for the average

specific heat. Three MDSC runs were carried out for each sample. The results of the DSC runs on all the samples and their analysis are presented in the Results and Discussion section.

3.5 Measurement of particle concentration - neutron activation analysis

The gross nature of the settling of nanoparticles in the base material due to gravitational effects is measured by the concentration gradient along the height of the test cylinder. The concentration of the nanoparticles is measured using neutron activation analysis. The method is suitable for the qualitative and quantitative analysis of minor and trace elements. The sample to be analyzed is bombarded with neutrons to create radioactive isotopes, which decay and emit measureable radiation--in our case gamma rays. The gamma ray emitted is characteristic of specific elements. We can analyze the signal to determine the concentration of a particular element--in our case, aluminum. The percentage mass concentration of the nanoparticles can be derived from the elemental percentage concentration.

$$Al^{27} + n^{1} \rightarrow Al^{28*}$$

$$Al^{28*} \rightarrow Al^{28} + \gamma \text{ (radiation)}$$

Al^{28}* - Radioactive isotope of aluminum

The sample from each zone of the test cylinder is analyzed using NAA, and the concentration of the nanoparticles in the top, middle and bottom zones is measured.

The neutron activation method was employed for quantitative analysis of aluminum in the sample, from which the percentage of alumina has been calculated. To check for neutron flux alteration due to the presence of lithium, standards were made on lithium carbonate substrate. 500 micro liters of 1000 µg/ml solution of aluminum oxide standards were deposited onto lithium. Three such standards were tested and gave results of 1056, 1045, and 1049 ppm (µg/g)

as against the expected results of 1000 ppm. There was a 5% positive bias, and it was surmised that the data did not indicate that any effect due to lithium was detected. The samples for the tests were made completely moisture-free and then deposited into 1 ml vials. The results of the tests give us the percentage of aluminum in the sample expressed as µg/g of aluminum. From this the percentage by mass of alumina is calculated using the formula:

$$\text{Mass percentage of alumina} = \frac{Mass\ of\ aluminum * 101.96\ )}{53.96} * 10^{-4} \qquad [5]$$

All the tests were carried out by the Center for Chemical Characterization and Analysis, Texas A&M University.

4. RESULTS AND DISCUSSION

This section presents the results of the neutron activation analysis and the DSC runs that were conducted on material before and after thermal cycling. As described above, there are 4 batches of material each of which undergoes a different number of thermal cycles. Batch A undergoes 1 thermal cycle, Batch B undergoes 20 thermal cycles, Batch C undergoes 40 thermal cycles and Batch D undergoes 60 thermal cycles. Each batch has 3 samples, so there are a total of 12 samples tubes in all. Each of these sample tubes has a top, middle and bottom section, from which material for analysis is taken. The starting material for the work was prepared in 6 batches with each batch containing 10 g of material. The concentration of alumina and the specific heat of each batch were measured to determine the variation in properties within the batches themselves.

4.1 Specific heat of the plain carbonate

The specific heat of the plain carbonate eutectic (without any nanoparticles) was measured. The specific heat of the plain material is measured by following the same MDSC temperature profile that was used for the enhanced samples.

The plot of the measured value compared to the theoretical values obtained using equation [1] is shown in Figure 9.

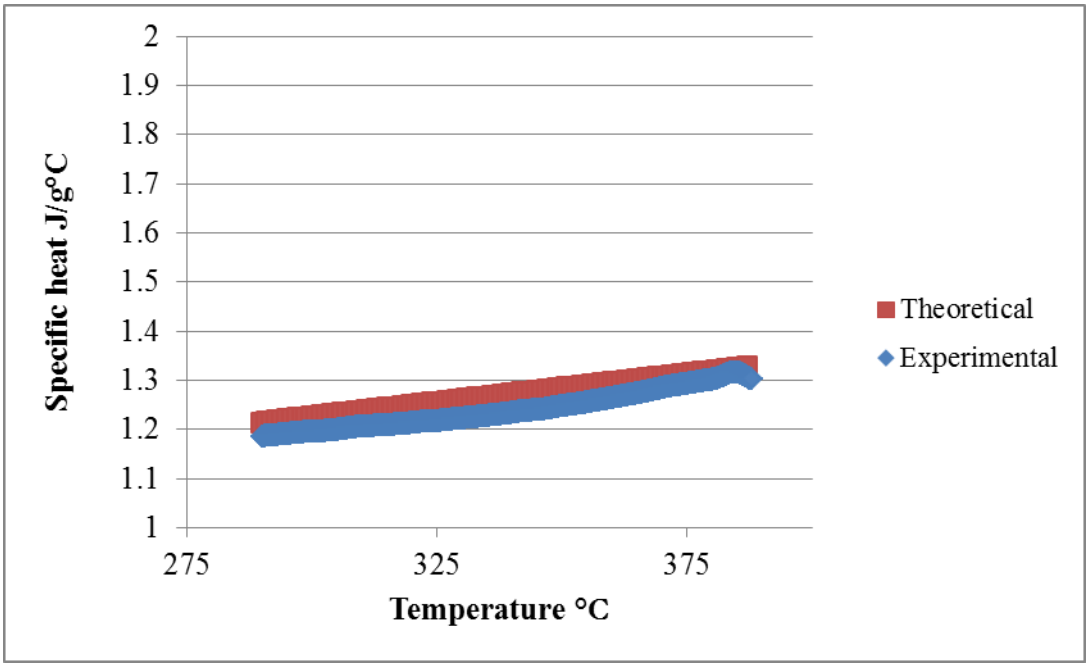

Figure 9 : Comparison between specific heat of plain carbonate measured using the MDSC method and the theoretical values

4.2 Original uncycled material

4.2.1 Concentration of alumina in the original uncycled material

Table 3 shows the mass percentage of alumina present in each of the 6 batches of the original uncycled material, measured using neutron activation analysis. The average mass percentage of the nanoparticles in the starting material is 0.96% with a standard deviation of 0.13%.

Table 3 : Concentration of alumina in the uncycled material

Batch	Alumina%	Std Dev
Batch 1	0.91	0.02
Batch 2	0.92	0.08
Batch 3	0.85	0.02
Batch 4	0.99	0.03
Batch 5	1.22	0.11
Batch 6	0.89	0.11

4.2.2 Specific heat of the original uncycled material

The specific heat of the original material is measured using the MDSC method, following the temperature profile described in the experimental procedure section.A typical MDSC run result is shown in Figure 10. The observed value of the specific heat of the original uncycled material is given in Table 4. The average specific heat is 1.38 J/g°C with a standard deviation of 0.15 J/g°C. The properties of the original uncycled material are the reference values to which the properties post-thermal cycling are compared. Therefore it is important to establish these values in the beginning.

Table 4 : Average specific heat of material in each batch of original uncycled material

	Average Specific heat (J/g°C)	
Sample	Average	Std Dev
Batch 1	1.60	0.53
Batch 2	1.32	0.12
Batch 3	1.20	0.17
Batch 4	1.23	0.24
Batch 5	1.31	0.21
Batch 6	1.53	0.29

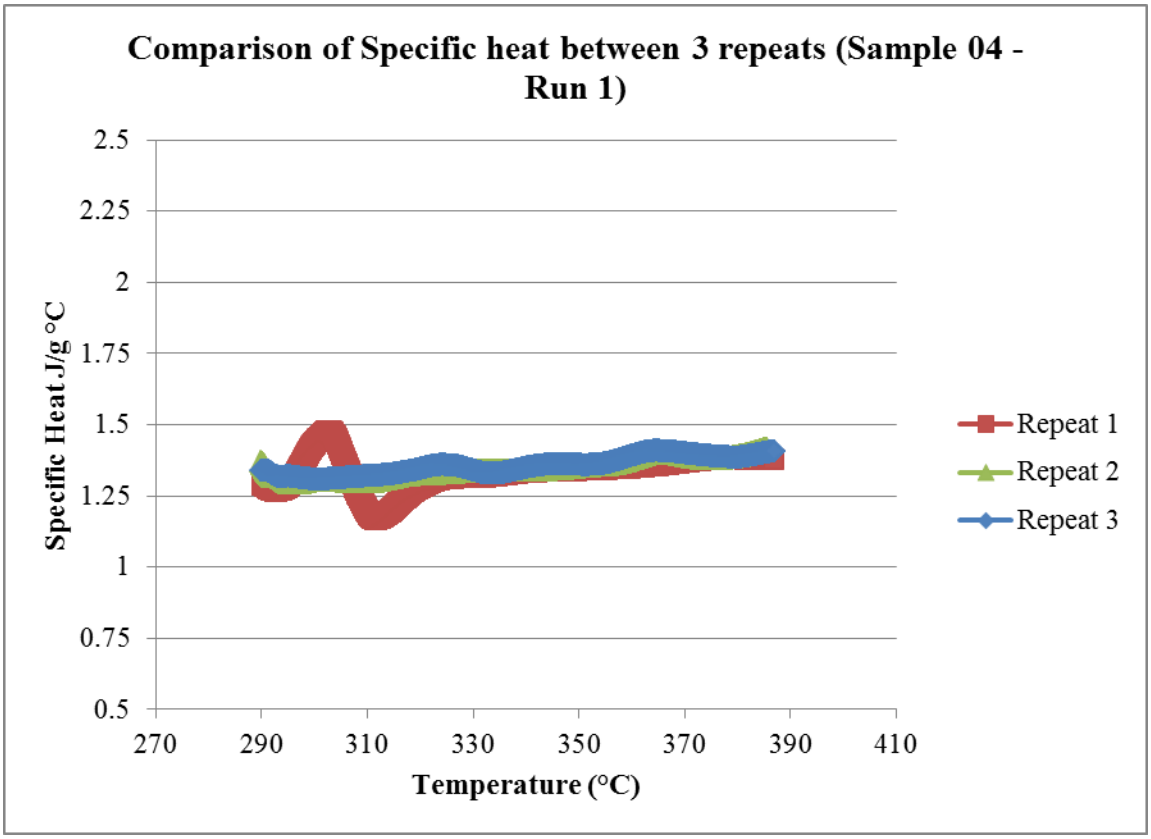

Figure 10 : Results of a typical MDSC run showing the 3 repeats

4.3 Properties of material post - thermal cycling

The materials undergo thermal cycling in a temperature-controlled furnace. The temperature profile and the process in which the thermal cycling is carried out are described in section 3. Each batch of thermally cycled material has 3 sample tubes and each sample tube is sectioned into 3 parts – top, middle and bottom. Specimen material taken from each of the sections is tested using neutron activation and subjected to the DSC runs. The average values measured by subjecting 3 specimens to each test is presented next.

4.3.1 Stability of nanocomposite with thermal cycling

The mass percentage of alumina is measured in the material taken from the central portion of the section and also from the portion near the wall of each section. The average mass percentage of alumina in the central portion of each section is listed in the Table 5. The mean and standard deviation of the concentration of alumina in each section is also given. The batch number in the parentheses indicates the source of the starting material of each sample.

Table 6 shows the mass percentage of alumina in the material taken from the portion near the wall in each section. (Not enough material could be recovered near the wall from the top section of Sample 7, so that place in the table has been left blank.) The values given are the average percentage of alumina by mass in each section.

Table 5 : Mass percentage of alumina in the thermally cycled material (material taken from the central portion of the sections)

		Mass percentage of alumina in the sample					
No of thermal cycles	Sample	Top		Middle		Bottom	
		Average	Std Dev	Average	Std Dev	Average	Std Dev
1	Sample 1 (Batch 1)	0.21	0.15	1.6	0.048	2.04	0.026
	Sample 2 (Batch 1)	0.053	0.0080	1.7	0.038	1.9	0.083
	Sample 3 (Batch 2)	0.026	0.0020	0.24	0.14	2.2	0.15
20	Sample 4 (Batch 2)	0.18	0.11	0.0060	0.0020	0.015	0.0070
	Sample 5 (Batch 3)	0.016	0.0010	0.024	0.0030	0.018	0.0020
	Sample 6 (Batch 3)	0.022	0.0010	0.024	0.0070	0.022	0.0010
40	Sample 7 (Batch 4)	0.012	0.0020	0.0050	0.0010	0.56	0.13
	Sample 8 (Batch 4)	0.030	0.013	0.011	0.0030	0.21	0.065
	Sample 9 (Batch 5)	0.028	0.018	0.016	0.0020	0.016	0.0010
60	Sample 10 (Batch 5)	0.0090	0.0040	0.016	0.0010	0.026	0.0020
	Sample 11 (Batch 6)	0.010	0.0020	0.0040	0.0010	0.053	0.043
	Sample 12 (Batch 6)	0.023	0.015	0.016	0.0010	0.069	0.027

Table 6 : Mass percentage of alumina in the thermally cycled material (material taken from near the wall of the sections)

		Mass percentage of alumina in the sample near wall					
No of thermal cycles	Sample	Top		Middle		Bottom	
		Average	Std Dev	Average	Std Dev	Average	Std Dev
1	Sample 1 (Batch 1)	0.44	0.019	0.59	0.36	0.39	0.24
	Sample 2 (Batch 1)	0.21	0.049	0.96	0.038	1.3	0.098
	Sample 3 (Batch 2)	0.030	0.0040	0.13	0.010	1.6	0.20
20	Sample 4 (Batch 2)	0.031	0.0040	0.0070	0.0020	0.96	0.47
	Sample 5 (Batch 3)	0.051	0.026	0.015	0.0040	0.49	0.20
	Sample 6 (Batch 3)	0.019	0.020	0.0090	0.0010	0.18	0.16
40	Sample 7 (Batch 4)	NA	NA	0.11	0.0050	2.7	0.73
	Sample 8 (Batch 4)	0.32	0.18	0.061	0.0050	3.7	0.27
	Sample 9 (Batch 5)	0.27	0.15	0.64	0.37	4.7	0.32
60	Sample 10 (Batch 5)	0.98	0.21	0.021	0.0080	0.29	0.044
	Sample 11 (Batch 6)	1.3	0.62	0.024	0.0070	0.27	0.019
	Sample 12 (Batch 6)	0.018	0.0030	0.011	0.0010	0.89	0.54

The mass percentage in the central portion is compared to the average concentration of alumina in the original uncycled material, which is 0.96%. This is shown in Table 7. Similarly, the relative mass percentage of alumina in the portion near the wall is tabulated in Table 11.

The relative mass percentage of alumina in the material taken from the portion near the wall section to the mass percentage of alumina in the material taken from the central portion of the section is useful for studying the radial distribution and clustering of the nanoparticles. This value is tabulated in Table 11.

Table 7 : Mass percentage of alumina in the thermally cycled material relative to the mass percentage of alumina in the original uncycled material (material taken from the central portion of the section)

		Relative mass percentage of alumina		
No of thermal cycles	Sample	Top	Middle	Bottom
1	Sample 1 (Batch 1)	0.22	1.6	2.2
	Sample 2 (Batch 1)	0.055	1.7	2.06
	Sample 3 (Batch 2)	0.027	0.25	2.3
20	Sample 4 (Batch 2)	0.18	0.0060	0.016
	Sample 5 (Batch 3)	0.017	0.025	0.019
	Sample 6 (Batch 3)	0.023	0.024	0.023
40	Sample 7 (Batch 4)	0.012	0.0050	0.58
	Sample 8 (Batch 4)	0.031	0.011	0.22
	Sample 9 (Batch 5)	0.029	0.017	0.017
60	Sample 10 (Batch 5)	0.010	0.016	0.027
	Sample 11 (Batch 6)	0.010	0.0040	0.055
	Sample 12 (Batch 6)	0.024	0.016	0.072

Table 8 :Log Average of Mass percentage of alumina in the thermally cycled material relative to the mass percentage of alumina in the original uncycled material (material taken from the central portion of the section)

Number of thermal cycles	Log Average of relative percentage of alumina		
	Top	Middle	Bottom
1	0.07	0.88	2.18
20	0.04	0.02	0.02
40	0.03	0.01	0.13
60	0.01	0.01	0.05

Table 9 : Mass percentage of alumina in the thermally cycled material relative to the mass percentage of alumina in the original uncycled material (material taken from near the wall of the section)

		Relative mass percentage of alumina		
No of thermal cycles	Sample	Top	Middle	Bottom
1	Sample 1 (Batch 1)	0.46	0.62	0.41
	Sample 2 (Batch 1)	0.22	0.99	1.3
	Sample 3 (Batch 2)	0.031	0.14	1.6
20	Sample 4 (Batch 2)	0.032	0.0070	0.99
	Sample 5 (Batch 3)	0.053	0.015	0.51
	Sample 6 (Batch 3)	0.020	0.010	0.19
40	Sample 7 (Batch 4)	NA	0.12	2.8
	Sample 8 (Batch 4)	0.34	0.063	3.8
	Sample 9 (Batch 5)	0.28	0.67	4.9
60	Sample 10 (Batch 5)	1.02	0.022	0.29
	Sample 11 (Batch 6)	1.3	0.025	0.28
	Sample 12 (Batch 6)	0.019	0.011	0.93

Table 10 : Log Average of Mass percentage of alumina in the thermally cycled material relative to the mass percentage of alumina in the original uncycled material (material taken from near the wall of the section)

Number of thermal cycles	Log Average of relative percentage of alumina		
	Top	Middle	Bottom
1	0.15	0.44	0.95
20	0.03	0.01	0.46
40	0.31	0.17	3.74
60	0.29	0.02	0.42

Table 11 : Mass percentage of alumina in the portion near the wall relative to the mass percentage of alumina in the material taken from the central portion of the sections

		Relative mass percentage of alumina		
No of thermal cycles	Sample	Top	Middle	Bottom
1	Sample 1 (Batch 1)	2.09	0.39	0.19
	Sample 2 (Batch 1)	3.9	0.59	0.66
	Sample 3 (Batch 2)	1.2	0.56	0.70
20	Sample 4 (Batch 2)	0.17	1.1	64.0
	Sample 5 (Batch 3)	3.2	0.60	27.0
	Sample 6 (Batch 3)	0.86	0.40	8.3
40	Sample 7 (Batch 4)	NA	22.0	4.9
	Sample 8 (Batch 4)	11.0	5.7	17.0
	Sample 9 (Batch 5)	9.5	39.0	290.0
60	Sample 10 (Batch 5)	105.0	1.4	11.0
	Sample 11 (Batch 6)	134.0	5.9	5.05
	Sample 12 (Batch 6)	0.79	0.68	13.0

4.3.2 Specific heat of the thermally cycled material

The average specific heat of the thermally cycled material after each thermal cycle is presented in Tables 10, 11, 12 and 13. The average specific heat in each section of the sample after a specific number of thermal cycles is considered for analysis. The average specific heat is the specific heat taken over the temperature range of 290°C to 397°C.

Table 12 : Average specific heat (in J/g°C) of the material in Batch A (1 thermal cycle)

Batch A	**Sample 1**		**Sample 2**		**Sample 3**	
Section	**Average Specific Heat**	**Std Deviation**	**Average Specific Heat**	**Std Deviation**	**Average Specific Heat**	**Std Deviation**
Top	1.95	0.26	1.63	0.039	1.76	0.109
Middle	1.62	0.26	1.77	0.21	1.9	0.078
Bottom	1.80	0.105	1.92	0.091	1.61	0.14

Table 13: Average specific heat (in J/g°C) of the material in Batch B (20 thermal cycles)

Batch B	Sample 4		Sample 5		Sample 6	
Section	**Average Specific Heat**	**Std Deviation**	**Average Specific Heat**	**Std Deviation**	**Average Specific Heat**	**Std Deviation**
Top	2.10	0.075	1.98	0.37	1.92	0.13
Middle	1.9	0.13	1.8	0.25	1.94	0.031
Bottom	1.8	0.099	1.8	0.12	1.9	0.23

Table 14 : Average specific heat (in J/g°C) of the material in Batch C (40 thermal cycles)

Batch C	Sample 7		Sample 8		Sample 9	
Section	**Average Specific Heat**	**Std Deviation**	**Average Specific Heat**	**Std Deviation**	**Average Specific Heat**	**Std Deviation**
Top	2.3	0.14	1.9	0.11	1.99	0.087
Middle	1.8	0.31	1.7	0.11	1.9	0.061
Bottom	1.9	0.15	1.85	0.11	2.02	0.089

Table 15 : Average specific heat (in J/g°C) of the material in Batch D (60 thermal cycles)

Batch D	Sample 10		Sample 11		Sample 12	
Section	**Average Specific Heat**	**Std Deviation**	**Average Specific Heat**	**Std Deviation**	**Average Specific Heat**	**Std Deviation**
Top	1.95	0.27	1.99	0.16	1.9	0.014
Middle	1.6	0.26	1.88	0.13	1.7	0.063
Bottom	1.8	0.105	1.7	0.059	1.9	0.045

It is useful to compare the specific heat of the thermally cycled material with the specific heat of the uncycled material. This relative value is obtained by dividing the specific heat of the thermally cycled material by the specific heat of the uncycled material from the batch corresponding to the original starting material. This is presented in the tables below.

Table 16 : Average specific heat of the material relative to the thermally uncycled material (Batch A – 1 thermal cycle)

Batch A	Sample 1		Sample 2		Sample 3	
Section	Relative Average Specific Heat	Std Deviation	Relative Average Specific Heat	Std Deviation	Relative Average Specific Heat	Std Deviation
Top	1.2	0.26	1.01	0.039	1.3	0.11
Middle	1.007	0.26	1.1	0.21	1.4	0.078
Bottom	1.12	0.105	1.12	0.091	1.22	0.14

Table 17 : Average specific heat of the material relative to the thermally uncycled material (Batch B- 20 thermal cycles)

Batch B	Sample 4		Sample 5		Sample 6	
Section	Relative Average Specific Heat	Std Deviation	Relative Average Specific Heat	Std Deviation	Relative Average Specific Heat	Std Deviation
Top	1.59	0.074	1.64	0.37	1.59	0.132
Middle	1.41	0.13	1.47	0.25	1.62	0.031
Bottom	1.37	0.099	1.45	0.11	1.57	0.23

Table 18 : Average specific heat of the material relative to the thermally uncycled material (Batch C – 40 thermal cycles)

Batch C	Sample 7		Sample 8		Sample 9	
Section	Relative Average Specific Heat	Std Deviation	Relative Average Specific Heat	Std Deviation	Relative Average Specific Heat	Std Deviation
Top	1.83	0.14	1.57	0.11	1.52	0.087
Middle	1.44	0.31	1.39	0.11	1.45	0.061
Bottom	1.56	0.15	1.49	0.11	1.55	0.089

Table 19 : Average specific heat of the material relative to the thermally uncycled material (Batch D – 60 thermal cycles)

Batch D	Sample 10		Sample 11		Sample 12	
Section	**Relative Average Specific Heat**	**Std Deviation**	**Relative Average Specific Heat**	**Std Deviation**	**Relative Average Specific Heat**	**Std Deviation**
Top	1.49	0.26	1.306	0.16	1.22	0.014
Middle	1.24	0.27	1.23	0.13	1.12	0.063
Bottom	1.38	0.105	1.089	0.059	1.24	0.045

4.4 Correlation between concentration of nanoparticles and the specific heat of the nanomaterial

The influence of the concentration of the nanoparticles in the composite material on the specific heat is studied by correlating the specific heat in each section of the sample with the concentration of alumina in that section. The semi log plots of the average specific heat of the sample with the average concentration of alumina in the respective section are shown in Figures 11-14.The semi log plots of the relative average specific heat of the sample (relative to the specific heat of the uncycled material) with the concentration of the alumina is shown in Figures 15-18.

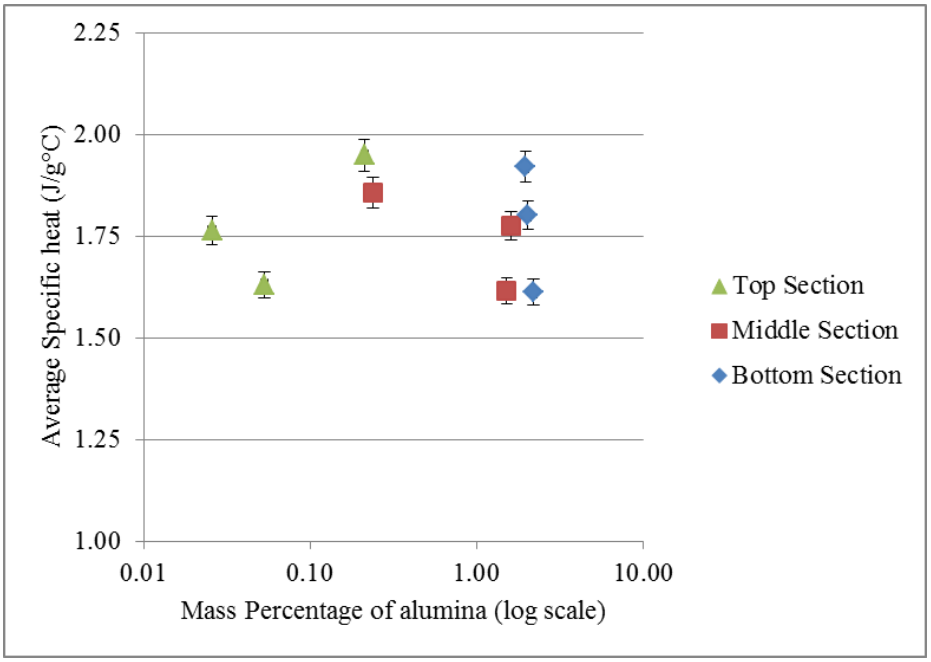

Figure 11 : Correlation between the average mass percentage and average specific heat in Batch A (1 thermal cycle)

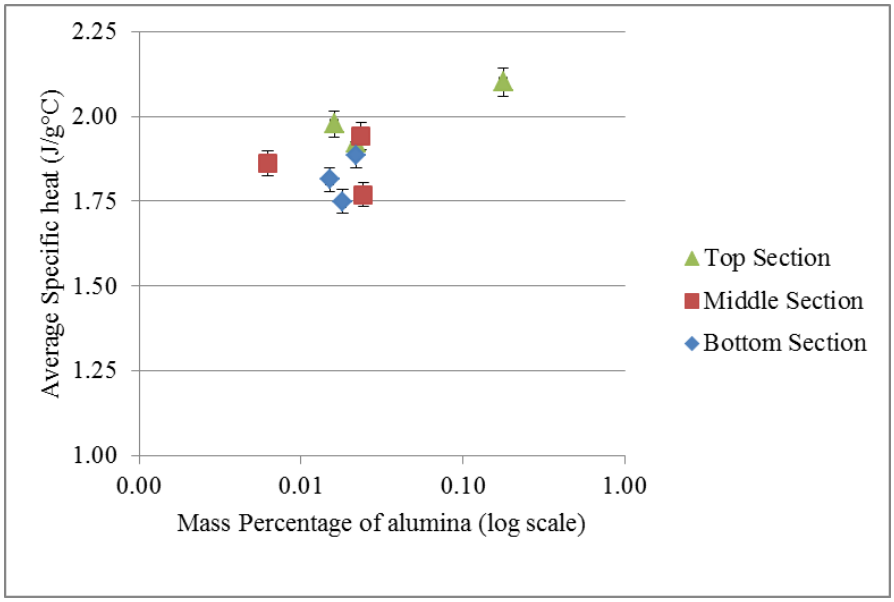

Figure 12: Correlation between the average mass percentage and average specific heat in Batch B (20 thermal cycles)

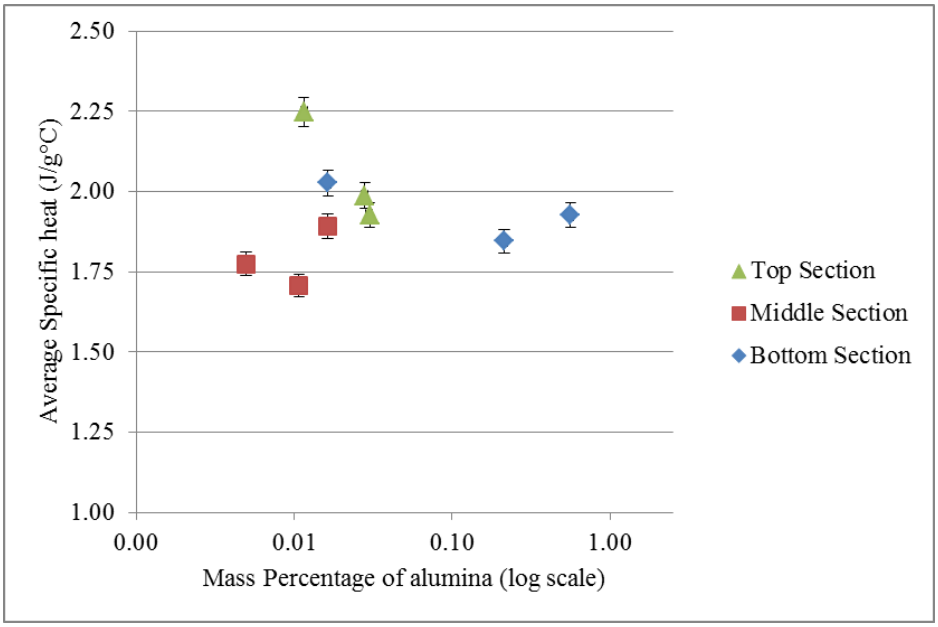

Figure 13 : Correlation between the average mass percentage and average specific heat in Batch C (40 thermal cycles)

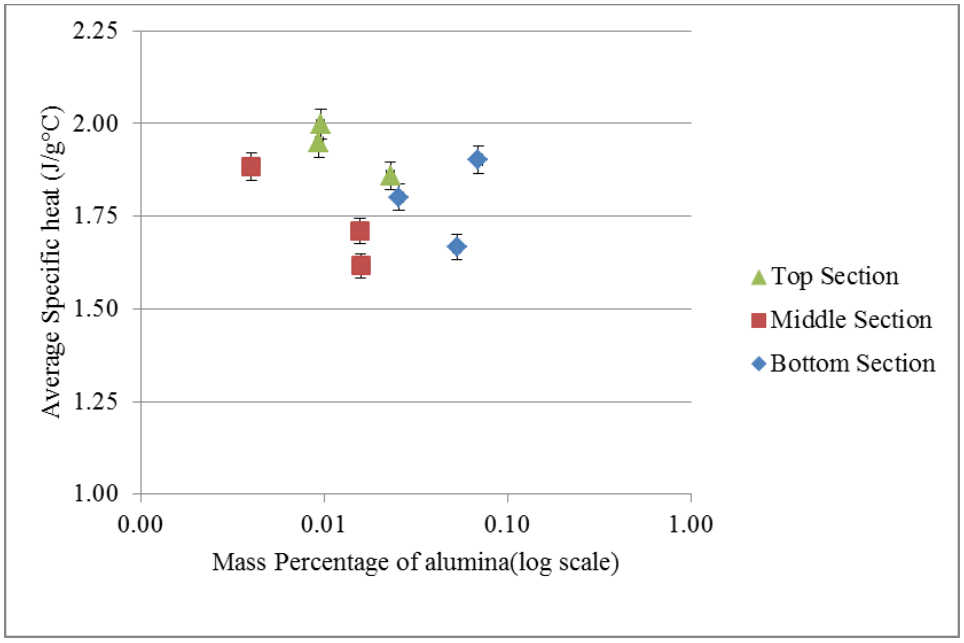

Figure 14 : Correlation between the average mass percentage and average specific heat in Batch D (60 thermal cycles)

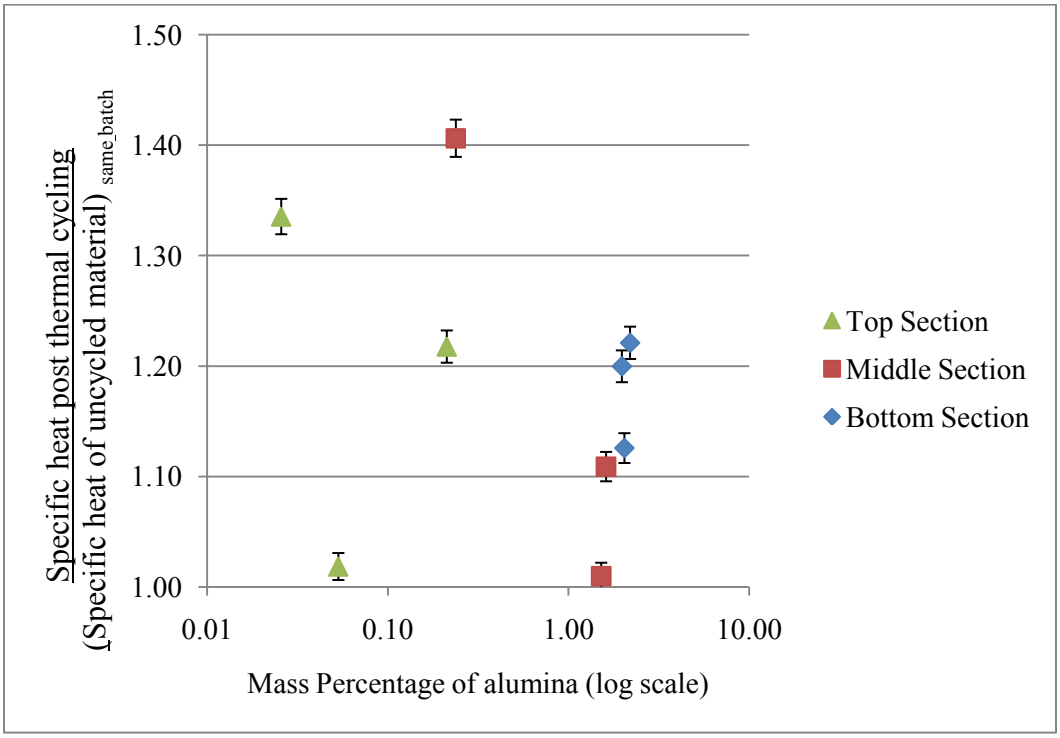

Figure 15 : Correlation between the average mass percentage and relative average specific heat in Batch A (1 thermal cycle)

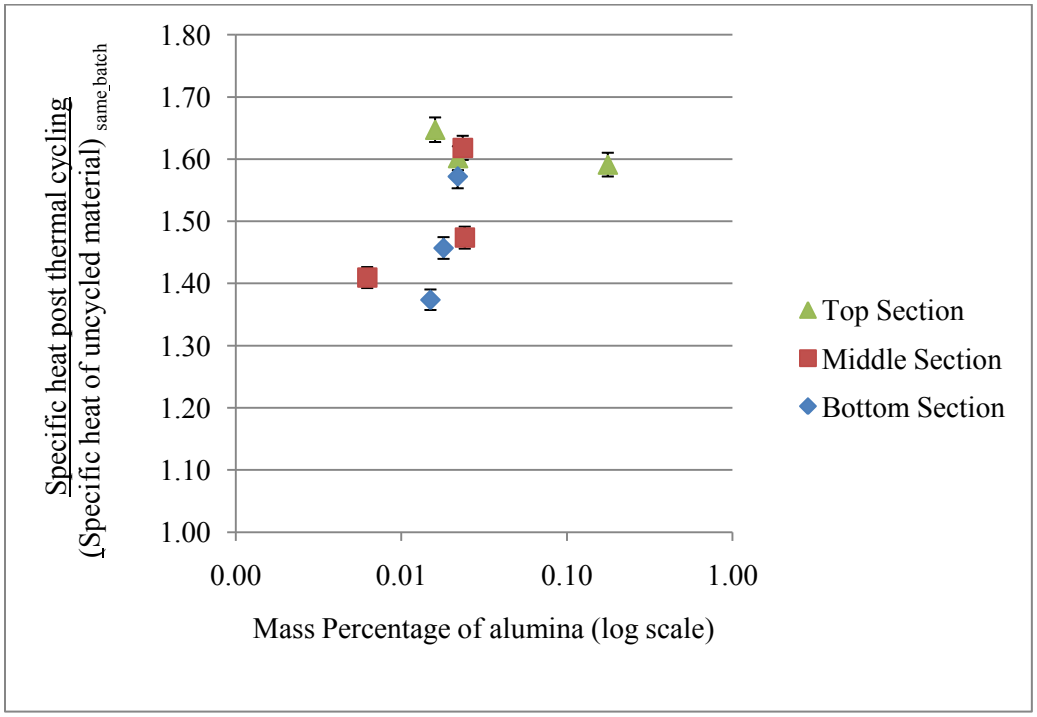

Figure 16 : Correlation between the average mass percentage and relative average specific heat in Batch B (20 thermal cycles)

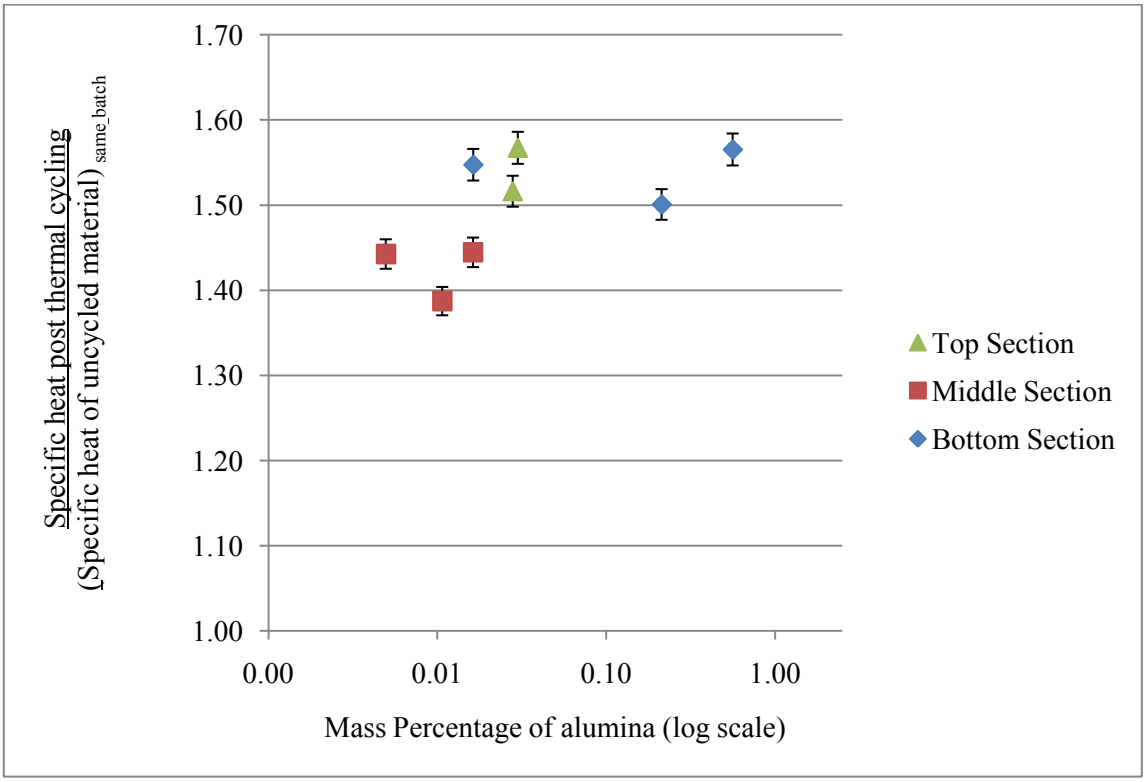

Figure 17 : Correlation between the average mass percentage and relative average specific heat in Batch C (40 thermal cycles)

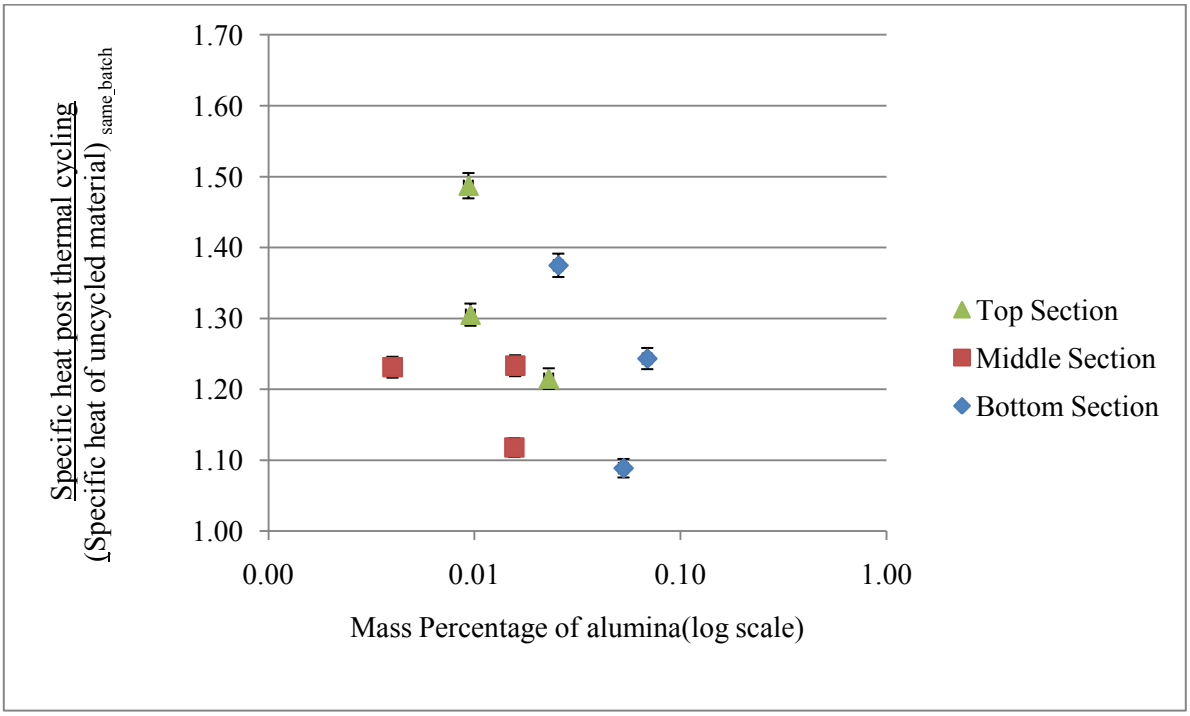

Figure 18 : Correlation between the average mass percentage and relative average specific heat in Batch D (60 thermal cycles)

5. DISCUSSION OF RESULTS

The results from the neutron activation test and the DSC which were presented in the previous section are discussed in this section. The specific heat of the uncycled material is discussed in the first section. This is followed by the discussion of the properties of the material post thermal cycling. This includes the specific heat of the material after thermal cycling and the distribution of nanoparticles in the material after thermal cycling. Finally the correlation between the concentration of alumina and the specific heat of the nanoparticles is considered in the last section.

5.1 Specific heat of original uncycled material

The average specific heat of the original uncycled material is given in Table 4. To determine an average specific heat, 3 specimen runs were conducted for each sample. Each MDSC run has 3 repeat runs which take place between 275°C and 410°C. A wide temperature range was selected to make up for any data loss when the MDSC parameters were triggered during the beginning of each repeat run. A typical result obtained from each MDSC run is shown in Figure 7. In Figure 7, the value of the specific heat in repeat 1 has an abrupt and irregular behavior. Such a jump occurs in the first repeat of the MDSC and tends to occur randomly. This jump in the specific heat can be attributed to irreversible geometric changes in the material when it undergoes the slow heating ramp during the first repeat of each run. The repeat 1 is not taken into account while calculating the average specific heat of each run. The values in repeat 2 and repeat 3 are generally in agreement with each other in most cases. The average specific heat of each run is the average of repeat 2 and repeat 3 of each DSC run between 290°C-387°C. The average specific heat is 1.38 J/g°C with a standard deviation of 0.15 J/g°C.

5.2 Properties of the nanomaterial - post thermal cycling

The specific heat of the nanomaterial and the stability of the nanoparticles in the carbonate eutectic are the two aspects of interest after the thermal cycling. The MDSC technique is used to measure the average specific heat of the nanocomposites, and neutron activation analysis is used to measure the average concentration of the nanoparticles. The results obtained were presented in the previous section, and a discussion of the results is presented next.

5.2.1 Stability of nanocomposite with thermal cycling

The mass percentage of alumina nanoparticles in each section of the sample material after thermal cycling is shown in Table 1. These values are within the 95% confidence interval. The samples in Batch A (Sample 1, Sample 2, Sample 3) indicate the settling of nanoparticles at the bottom of the sample tube. The material in Batch A has been held in the liquid state for only one hour, and the average concentration of the alumina nanoparticles in the sample taken from the bottom section of the tube is 2.07%. This is twice the average concentration of the nanoparticles in the original material. Within the 95% confidence interval, the top section has the least concentration of the nanoparticles, and the middle section has an intermediate value of nanoparticles by mass percentage. The Stokes model for the settling velocity for the nanoparticles estimated 20 hours for particles of a diameter of 20 microns to settle. However, the nanoparticles appear to settle considerably after the first thermal cycle itself. Such a disparity in the concentration is not found in Batch B, which undergoes 20 thermal cycles. Batch C and Batch D, which undergo 40 and 60 thermal cycles respectively, however, show a similar trend in the distribution of the nanoparticles along the height of the sample cylinder. This separation of the nanoparticles is not a desired characteristic. It is preferred that the nanoparticles remain homogeneously distributed throughout the sample even after the thermal cycles. The settling of the nanoparticles can be attributed to the large cluster size of the nanoparticles, as heavier

clusters settle towards the bottom. Although the concentration of the nanoparticles in the bottom section decreases with the number of the thermal cycles, the gradient still exists. Settling is not desirable in either a thermocline system or a two-tank system. The stability of the nanoparticles in any other molten salt is undesirable when used as an HTF also.

5.2.2. Dispersion of nanoparticles towards the wall

Another important observation is made by comparing the mass percentage of the alumina in the material taken from the central portion of the cylinder to the mass percentage of alumina in the material taken from near the walls; namely, the dispersion of the nanoparticles towards the wall of the sample tube.

The mass percentage of alumina in the samples in Batches B, C and D is less than the mass percentage of alumina in the samples in Batch A or even in the original uncycled material. This reduced concentration of alumina must be accounted for; therefore the material taken from the near the wall in each section was also tested using the neutron activation technique. The results of these tests are shown in Table 6. Firstly, the mass percentage of alumina in the material near the wall helps identify the reason the mass percentage of the sample in the central portion in Batches B, C, D is less than in Batch A. Secondly, the relative values of the mass percentage in the wall portion compared to the mass percentage in the central portion, which is shown in Table 11, shows that there is considerable wall effect on the material in the cylindrical sample holder. This is seen clearly in the top section, where the mass percentage is an order of magnitude higher than the material in the central section. In some cases, such as sample 10 and sample 11, the mass percentage is 100 times the mass percentage in the central portion. This effect is also seen in the middle and bottom sections, but it is not as dramatic as it is in the top section. The relative mass percentage value of the bottom portion of sample 9 is also an order of magnitude high.

The clustering of the nanoparticles near the wall is as much of a concern as the settling behavior due to gravity. From the relative mass percentage, it can be seen that after thermal cycles, there is a greater accumulation of nanoparticles towards the wall of the container than there is towards the bottom due to settling. Since the thermal conductivity of the nanofluids depends on the concentration of the nanoparticles (11), such a radial dispersion of the nanoparticles could vary the thermal conductivity of the nanofluid if it is used as a HTF in pipes.

The Stokes model used for calculating the settling velocity did not account for the wall's effect on the nanoparticles. The attractive force on the particles near the wall is greater than the attractive force on the particles in the central portion of the cylindrical tube. This drag force reduces the settling velocity of the particles near the wall and increases the accumulation of the particles near the walls. This effect can explain the increase in the relative mass percentage with the increase in the number of thermal cycles near the wall, especially in the top section of the sample tube.

The stability of the nanoparticles in the salt material is very important. The nanoparticles are expensive, and their addition to the nanocomposites is useless if they fall out during operation. This will require a system to ensure that they are homogeneously mixed within the nanocomposite, or else the lost nanoparticles have to be replenished, which is an expensive option.

The influence of this dispersion of the nanoparticles on the specific heat is discussed separately in this section. The specific heat of the thermally cycled material is discussed in the next section.

5.2.3 Specific heat of thermally cycled material

The specific heat of the thermally cycled material exhibits very interesting behavior. The average specific heat in each section of the sample in all the batches is presented in Tables 12, 13, 14, and 13. Also, the average specific heat relative to the specific heat of the uncycled material is shown in Tables 16, 17, 18, and 19. The values of the specific heat lie in the range of 1.6+-2.2 J/g°C. The value of the specific heat is not affected by the number of thermal cycles that the material has undergone. This stability in specific heat with an increase in the number of thermal cycles is one of the desirable traits of a TES material. This also indicates that there is no degradation in the material itself with the thermal cycling, as the specific heat remains uniformly in the same range after the thermal cycles.

Another aspect of the specific heat is seen in the relative average specific heat of the material when compared to the uncycled specific heat of the material. The average specific heat of the uncycled material is 1.38 J/g°C. The cycled material shows an enhancement of specific heat compared to the uncycled material. This enhancement is seen in Tables 16, 17, 18, 19, where the value varies between 1.2-1.8 J/g°C., this enhancement of specific heat is a good outcome of thermal cycling.

A third aspect of the specific heat is the correlation of the specific heat with the mass percentage of alumina in the material, which is discussed below.

5.2.4 Correlation between concentration of nanoparticles and the specific heat of the nanomaterial

Figures 8, 9, 10 and 11 plot the average specific heat against the average mass percentage of alumina in each batch of the material. The plots suggest there is no strict correlation between the concentration of the alumina and the specific heat of the material. This is seen in all 4 plots, where the variation in mass percentage of alumina within the section does not affect the specific heat of the material in that section. For example, the bottom section has the highest percentage of alumina, but this does not influence the specific heat of the material very much. Therefore, thermal cycling causes the nanoparticles to separate out and alters the distribution of the nanoparticles, but as a result of this variation in distribution there is no influence on the specific heat of the material. The plots between the average specific heat and the average mass percentage of the nanoparticles for each sample can be found in Appendix B. The plots for each of these sample tubes also exhibit the same behavior.

A second conclusion can be drawn from the section of the sample which has a very small concentration of nanoparticles. When observing of the specific heat of the material in the top section, we see that that even at a low concentration of alumina, the specific heat of the material is enhanced. However, an increase of concentration of nanoparticles in the bottom section does not result in a proportional increase of specific heat. This suggests that the enhancement of the specific heat of the material occurs at very low concentration. There is need for a better understanding of how the concentration of the nanoparticles influences the specific heat of the material in the solid state. It would be interesting to study the effect of the mass percentage of the nanoparticles when the nanoparticles are present in trace amounts. If the enhancement of the material can be achieved with a lesser concentration of nanoparticles, this would decrease the cost of the nanocomposite and also the overall system cost. However, the lower and the upper

limits of the concentration of the nanoparticles required for attaining an effective enhancement of the specific must be established first.

It can be confidently stated that the presence of nanoparticles enhances the specific heat of the bulk material but this enhancement is not directly proportional to the mass of the nanoparticles present .This fact will be useful in understanding the theory behind the nature of nanoparticles and why their presence influences the specific heat of the bulk material.

A possible explanation which can be speculated for the enhancement of specific heat at trace concentrations can be given by studying the structure and size of the nanoparticles in the sample. It has been established that the sample in the top section of the sample tube has enhanced specific heat even though it has lower concentration of alumina nanoparticles. The sample in the top section of the tube has a lower concentration of nanoparticles than the sample in the bottom section. It is possible that the nanoparticles in the bottom section tend to be large clusters of nanoparticles and the top section of the sample tube would be free of any clusters. The correlation between the size and the surface to volume ratio of the nanoparticle and the specific heat of the nanomaterial should be determined. If in fact the size and the surface to volume ratio of the nanoparticle play a crucial role in enhancing the specific heat of the nanomaterial then the enhancement of the material in top section can be explained by determining the size of nanoparticles in the material.

6. SUMMARY OF FINDINGS

1. The thermal cycling causes settling of nanoparticles due to gravity.
2. Thermal cycling causes the migration of the nanoparticles towards the walls of the sample container.
3. The specific heat of the thermally cycled nanomaterial is stable with thermal cycling and does not show any trend with cycling time. The specific heat of the nanomaterial after thermal cycling is higher than the specific heat of the uncycled material.
4. The specific heat of the nanomaterial is independent of the concentration of the nanoparticles in the material.
5. The specific heat of the nanomaterial is enhanced even at very low concentration of the nanoparticles in the nanomaterial.

.

7. CONCLUSIONS

- Thermal cycling changes the distribution of the nanoparticles in the composite material;
- This change in the concentration of alumina does not appear to affect the specific heat of the material for our test conditions.

8. RECOMMENDATIONS FOR FUTURE WORK

The current study has been carried out for a maximum of 60 thermal cycles. Although the specific heat of the material does not change drastically with thermal cycling, it would be interesting to see if there is such a change with increased number of thermal cycles. This will definitely establish confidence in using the material in an actual TES system.

The effect of the concentration of the nanoparticles at trace concentrations should be further explored. The upper and lower limits for enhancing the specific heat of the nanomaterial would be useful information that could enable manufacture of the nanomaterial at a lower cost.

A better model for predicting the migration of the nanoparticles, that takes the wall's effect into account, eventually has to be developed in order to control the dispersion of the nanoparticles in nanofluids.

Finally, all the measurements pertaining to thermal property work have been carried out by studying the specific heat of the material in the solid state. It would be useful to study the heat of fusion and the specific heat of the material in the liquid state and explore the changes in these properties with thermal cycling.

REFERENCES

1. Owens, B., 2003, "The Value of Thermal Energy Storage," Workshop on Thermal Storage for Trough Power Systems, Boulder, CO, Feb. 20-21, 2003.

2.Herrmann, U., Kearney, D.W., 2002, "Survey of Thermal Energy Storage for Parabolic Trough Power Plants," Journal of Solar Energy Engineering, **124**, pp. 145-153.

3. Gil, A., Medrano, M., Martorell, I., La´zaro, A., Dolado, P., Zalba, B., 2010, "State of the Art on High Temperature Thermal Energy Storage for Power Generation," Renewable and Sustainable Energy Review," **14**, pp. 31-55.

4. Gil, A., Medrano, M., Martorell, I., La´zaro, A., Dolado, P., Zalba, B., 2010, "State of the Art on High Temperature Thermal Energy Storage for Power Generation," Renewable and Sustainable Energy Review ," **14**, pp. 56-72.

5. Pacheco., 2001, "Demonstration of solar-generated electricity on demand: the solar two project," Journal of Solar Energy Engineering –Transactions of the ASME 2001, **123**, pp. 153-158.

6. Pacheco, J., Steven, K., Kolb, W.J., 2002, "Development of a Molten Salt Thermocline Thermal Storage System for Parabolic Trough Plants," Journal of Solar Energy Engineering, **124**, pp. 153-160.

7. Petri, R.J., 1979, "Evaluation of Molten Carbonates as Latent Heat Thermal Energy Storage materials," Proceedings of the 14th Intersociety Energy Conversion Engineering Conference, Boston, MA, Aug. 5-10, 1979.

8. Janz, G.J., Allen, C.B., Bansal, N.P., Murphy, R.M., Tomkins, R.P.T., 1979 " Physical Properties Data Compilation Relevant to Energy Storage, Molten Salt: Data on Single and Multi

Component Salt Systems," National Standard Reference Data System, National Bureau of Standards, 61, Part I.

9.Araki, N., Matsuura, M., Makino, M., Hirata, T., and Kato, Y., 1988, "Measurement of Thermophysical Properties of Molten Salts: Mixture of Alkaline Carbonate Salts," International Journal of Thermophysics, **9**, pp.1071-1080.

10. Sheikh, S., Lafdi, K.,Hallinan, K., 2008, "Carbon Nanoadditives to Enhance Latent Energy Storage," Journal of Applied Physics, **103**, pp.3538-3544.

11. Stephen, C., Eastman, J.A., 1995, "Enhancement of Thermal Conductivity of Fluids with the Addition of Nanoparticles," Development and Application of Non-Newtonian Fluids, **231**, pp. 99-105.

12. Sheng, N., Rui, Z.,2008, "Measurement of the Specific Heat Capacity of Water-Based Al2O3 Nanofluid," Applied Physics Letters, **92**, pp. 2008-2010.

13. Xuan, Y., Roetzal, W., 2009, "Conceptions for Heat Transfer Correlations," International Journal of Heat and Mass Transfer, **43**, pp. 3701-3707.

14. Vajjha, K., Das, D. K., 2009, "Specific Heat Measurement of Three Nanofluids and Development of a New Correlation," International Journal of Heat Transfer, **131**, pp. 071601 1-5.

15. Shukla, A., Buddhi, D., Sawhney, R.L., 2008, "Thermal Cycling Test of Few Selected Inorganic and Organic," Renewable Energy, **33**, pp. 2606-2614.

16. Sari, A., 2003, "Thermal Reliability Test of Some Fatty Acids as PCMs used for Solar Thermal Latent Heat Storage Applications," Energy Conversion and Management, **44**, pp. 2277-2287.

17.Dimitrijevic, N.M., 1999, “Charge Separation across the Silica Nanoparticle/Water Interface,” Journal of Physical Chemistry, **103**, pp. 9533-9539.

18. TA Instruments, "Modulated Differential Scanning Calorimetry – Theory," Thermal Analysis and Rheology, TA-211B, http://www.tainst.com. Date last accessed, May 12, 2011.

APPENDIX A

RAW DATA OBTAINED FROM NEUTRON ACTIVATION ANALYSIS

Sample ID	Mass	Al (ug/g)	Smp Avg (ug/g)	Reported (ug/g)	Smp STD (ug/g)	Smp RSTD (%)
IT	0.41010	2016	1124	1100	795	70.73
IT	0.03366	492				
IT	0.03413	863				
IM	0.04024	7983	8033	8000	255	3.18
IM	0.04173	8310				
IM	0.04280	7807				
IB	0.03641	10690	10797	10800	136	1.26
IB	0.04212	10950				
IB	0.03896	10750				
IIT	0.04400	290	282	280	43	15.30
IIT	0.04882	320				
IIT	0.03679	235				
IIM	0.03116	8467	8548	8500	201	2.36
IIM	0.02947	8777				
IIM	0.03496	8399				
IIB	0.03457	10010	10453	10500	440	4.21
IIB	0.03339	10460				
IIB	0.03211	10890				
IIIT	0.03485	140	136	140	10	7.09
IIIT	0.03601	125				
IIIT	0.04420	143				
IIIM	0.03655	1360	1514	1500	754	49.79
IIIM	0.04202	2333				
IIIM	0.03501	849				
IIIB	0.03842	10780	11557	11600	770	6.66
IIIB	0.03579	12320				
IIIB	0.04091	11570				

Neutron Activation Analysis results on material taken from the central portion of Batch A.

Sample ID	Mass	Al (ug/g)	Smp Avg (ug/g)	Reported (ug/g)	Smp STD (ug/g)	Smp RSTD (%)
IV B	0.03229	1358	937	900	565	60.37
IV B	0.03043	1158				
IV B	0.02970	294				
IV M	0.03439	28.2	33	30	8	24.63
IV M	0.02932	28.3				
IV M	0.02698	42.3				
IV T	0.02776	96.4	77	80	36	46.25
IV T	0.03899	98.2				
IV T	0.03339	35.8				
V B	0.03131	82	95	100	13	13.19
V B	0.03288	107				
V B	0.03324	96.4				
V M	0.03096	141	128	130	17	13.14
V M	0.02927	134				
V M	0.02724	109				
V T	0.02776	91.5	84	80	7	7.80
V T	0.02800	82				
V T	0.02867	78.9				
VI B	0.02836	113	114	110	6	5.30
VI B	0.03048	120				
VI B	0.03433	108				
VI M	0.02950	93.3	124	120	36	29.01
VI M	0.02743	164				
VI M	0.02878	116				
VI T	0.03089	113	116	120	7	6.03
VI T	0.02718	124				
VI T	0.03140	111				

Neutron Activation Analysis results on material taken from the central portion of Batch B.

Sample ID	Mass	Al (ug/g)	Smp Avg (ug/g)	Reported (ug/g)	Smp STD (ug/g)	Smp RSTD (%)
VII B	0.00133	3717	2966	3000	676	22.78
VII B	0.01671	2775				
VII B	0.01413	2407				
VII M	0.01377	19.85	26.25	26	6	21.18
VII M	0.01531	29.89				
VII M	0.01787	29.01				
VII T	0.01297	51.28	60.95	61	13	21.40
VII T	0.01469	55.78				
VII T	0.01683	75.78				
VIII B	0.01816	926	1126	1100	342	30.33
VIII B	0.02036	932.4				
VIII B	0.01570	1521				
VIII M	0.01188	74.43	56.66	57	16	27.68
VIII M	0.01553	50.79				
VIII M	0.01620	44.76				
VIII T	0.01470	243.3	161.4	160	71	43.96
VIII T	0.01410	118.7				
VIII T	0.01556	122.2				
IX B	0.01333	80.15	86.47	87	6	6.40
IX B	0.01416	88.78				
IX B	0.01884	90.47				
IX M	0.01870	77.34	86.22	86	8	9.65
IX M	0.01646	93.84				
IX M	0.01677	87.48				
IX T	0.01489	129.7	148.5	150	93	62.75
IX T	0.01345	249.6				
IX T	0.01748	66.13				

Neutron Activation Analysis results on material taken from the central portion of Batch C.

Sample ID	Mass	Al (ug/g)	Smp Avg (ug/g)	Reported (ug/g)	Smp STD (ug/g)	Smp RSTD (%)
X T	0.01224	48.73	49.58	50	20	39.77
X T	0.01638	30.3				
X T	0.01137	69.71				
X M	0.01331	90.08	83.56	84	6	7.01
X M	0.01401	81.86				
X M	0.01632	78.74				
X B	0.01276	145.7	135.40	135	9	6.83
X B	0.01151	132.7				
X B	0.01361	127.8				
XI T	0.01195	37.13	50.69	51	12	24.41
XI T	0.01382	61.37				
XI T	0.01114	53.57				
XI M	0.01268	24.03	21.21	21	5	21.61
XI M	0.01166	15.92				
XI M	0.01252	23.67				
XI B	0.01161	42.64	278.45	280	227	81.43
XI B	0.01277	494.9				
XI B	0.01454	297.8				
XII T	0.01680	74.12	121.56	120	79	65.09
XII T	0.01691	77.66				
XII T	0.01013	212.9				
XII M	0.01708	90.14	82.76	83	8	9.56
XII M	0.01920	83.74				
XII M	0.01946	74.4				
XII B	0.01230	522.5	365.93	370	141	38.62
XII B	0.02234	327.5				
XII B	0.01818	247.8				

Neutron Activation Analysis results on material taken from the central portion of Batch D.

Sample ID	Al (ug/g)	Smp Avg (ug/g)	Reported (ug/g)	Smp STD (ug/g)	Smp RSTD (%)
IT	2409	2343.67	2340	98	4.18
IT	2391				
IT	2231				
IM	911.7	3129.23	3000	1924	61.48
IM	4125				
IM	4351				
IB	3839	2097.33	2000	1512	72.07
IB	1127				
IB	1326				
IIT	899.1	1094.87	1100	261	23.83
IIT	1391				
IIT	994.5				
IIM	5238	5061.00	5100	201	3.98
IIM	4842				
IIM	5103				
IIB	7027	6846.67	6800	518	7.56
IIB	7250				
IIB	6263				
IIIT	140.6	159.73	160	20	12.52
IIIT	180.5				
IIIT	158.1				
IIIM	678.1	701.00	700	52	7.38
IIIM	664.7				
IIIM	760.2				
IIIB	9114	8145.67	8100	1061	13.03
IIIB	7011				
IIIB	8312				

Neutron Activation Analysis results on material taken from the wall portion of Batch A.

Sample ID	Al (ug/g)	Smp Avg (ug/g)	Reported (ug/g)	Smp STD (ug/g)	Smp RSTD (%)
IVT	179.9	162.47	160	24	14.58
IVT	135.5				
IVT	172				
IVM	30.33	37.45	37	12	31.93
IVM	30.76				
IVM	51.25				
IVB	7693	5064.67	5000	2476	48.90
IVB	4726				
IVB	2775				
VT	209	270.40	270	136	50.41
VT	175.6				
VT	426.6				
VM	64.3	77.32	77	24	30.68
VM	104.7				
VM	62.95				
VB	3846	2614.00	2600	1067	40.82
VB	1993				
VB	2003				
VIT	82.57	102.87	100	53	51.96
VIT	62.54				
VIT	163.5				
VIM	53.2	49.59	50	5	10.51
VIM	51.96				
VIM	43.62				
VIB	1894	961.63	1000	832	86.57
VIB	698				
VIB	292.9				

Neutron Activation Analysis results on material taken from the wall portion of Batch B.

Sample ID	Al (ug/g)	Smp Avg (ug/g)	Reported (ug/g)	Smp STD (ug/g)	Smp RSTD (%)
VIIM	600.6	583.93	580	28	4.78
VIIM	551.7				
VIIM	599.5				
VIIB	14505	14454.00	14000	3857	26.68
VIIB	18285				
VIIB	10572				
VIIIT	1656		1700		
VIIIM	291.1	320.90	320	26	8.14
VIIIM	339.9				
VIIIM	331.7				
VIIIB	19827	19444.00	19400	1437	7.39
VIIIB	20651				
VIIIB	17854				
IXT	1400		1400		
IXM	3421		3400		
IXB	26767	24844.33	24800	1667	6.71
IXB	23810				
IXB	23956				

Neutron Activation Analysis results on material taken from the wall portion of Batch C.

Sample ID	Al (ug/g)	Smp Avg (ug/g)	Reported (ug/g)	Smp STD (ug/g)	Smp RSTD (%)
XT	5755	5186.33	5200	1111	21.42
XT	5898				
XT	3906				
XM	38.53	88.11	90	44	49.70
XM	104.3				
XM	121.5				
XB	1656	1511.00	1500	232	15.38
XB	1634				
XB	1243				
XIT	5934	8646.00	9000	3305	38.22
XIT	12327				
XIT	7677				
XIM	84.09	125.10	130	38	30.02
XIM	133.4				
XIM	157.8				
XIB	1536	1417.67	1420	103	7.27
XIB	1347				
XIB	1370				
XIIT	83.27	96.58	97	17	17.96
XIIT	90.28				
XIIT	116.2				
XIIM	47.18	55.89	56	8	13.68
XIIM	59.03				
XIIM	61.47				
XIIB	1857	4732.33	5000	2864	60.52
XIIB	7585				
XIIB	4755				

Neutron Activation Analysis results on material taken from the wall portion of Batch D.

APPENDIX B

MODULATED DSC RESULTS AND CORRELATION WITH THE SPECIFIC HEAT FOR EACH SAMPLE TUBE

Batch A- (1 thermal cycle) Sample 1

		Specific heat J/g°C		
Section	**Specimen**	**Average of cycle 2 and cycle 3**	**Average of runs for each section**	**Std Deviation of runs for each section**
Top	1	2.2523	1.9481	0.2647
	2	1.7700		
	3	1.8222		
Middle	1	1.9173	1.6156	0.2648
	2	1.4221		
	3	1.5073		
Bottom	1	1.6836	1.8011	0.1050
	2	1.8859		
	3	1.8337		

Percentage of alumina			
Alumina %	**Average %**	**Reported %**	**STD**
0.7619	0.4246	0.4157	0.3003
0.1859			
0.3261			
3.0169	3.0359	3.0233	0.0965
3.1404			
2.9503			
4.0399	4.0802	4.0814	0.0514
4.1381			
4.0625			

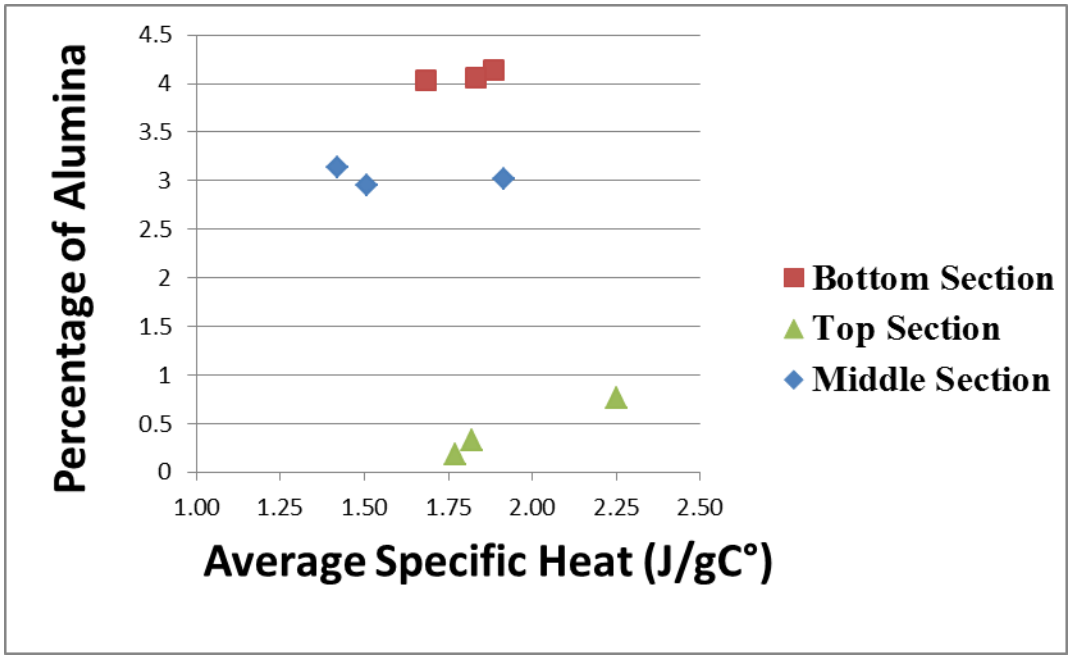

Graph correlating the concentration of nanoparticles with the specific heat in Batch A (Sample 1).

Batch A - (1 thermal cycle) Sample 2

		Specific heat J/g°C		
Section	Specimen	Average of cycle 2 and cycle 3	Average of runs for each section	Std Deviation of runs for each section
Top	1	1.6500	1.6295	0.0390
	2	1.5845		
	3	1.6539		
Middle	1	1.8770	1.7742	0.2111
	2	1.5315		
	3	1.9143		
Bottom	1	1.9047	1.9196	0.0910
	2	2.0172		
	3	1.8370		

Percentage of alumina			
Alumina %	Average %	Reported %	Smp STD
0.110 0.121 0.089	0.106	0.106	0.016
3.200 3.317 3.174	3.230	3.212	0.076
3.783 3.953 4.115	3.950	3.968	0.166

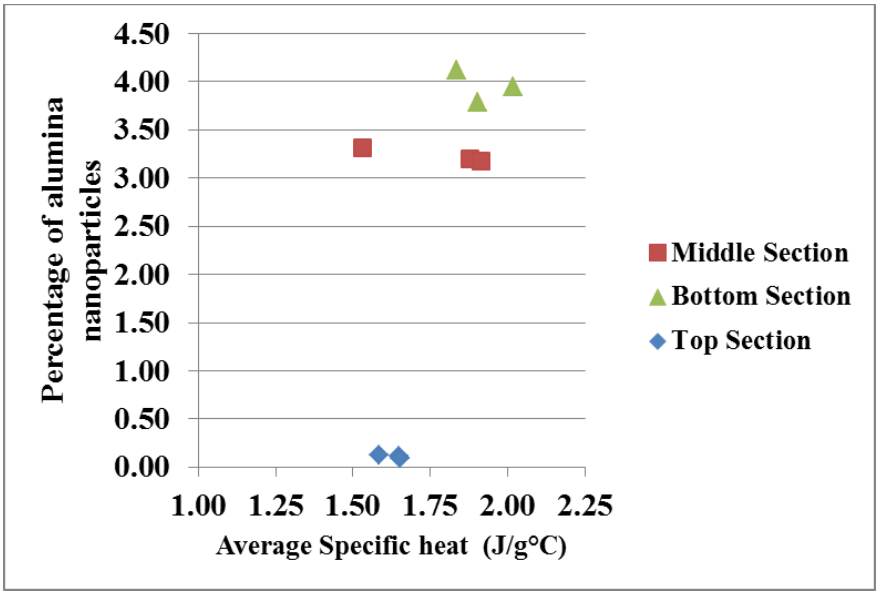

Graph correlating the concentration of nanoparticles with the specific heat in Batch A (Sample 2).

Batch A - (1 thermal cycle) Sample 3

		Specific heat J/g°C		
Section	**Specimen**	**Average of cycle 2 and cycle 3**	**Average of runs for each section**	**Std Deviation of runs for each section**
Top	1	1.8507	1.7627	0.1093
	2	1.7970		
	3	1.6403		
Middle	1	1.7794	1.8563	0.0778
	2	1.9350		
	3	1.8545		
Bottom	1	1.7069	1.6117	0.1396
	2	1.6768		
	3	1.4514		

Percentage of alumina			
Alumina %	**Average %**	**Reported %**	**Smp STD**
0.053	0.051	0.053	0.004
0.047			
0.054			
0.514	0.572	0.567	0.285
0.882			
0.321			
4.074	4.367	4.384	0.291
4.656			
4.372			

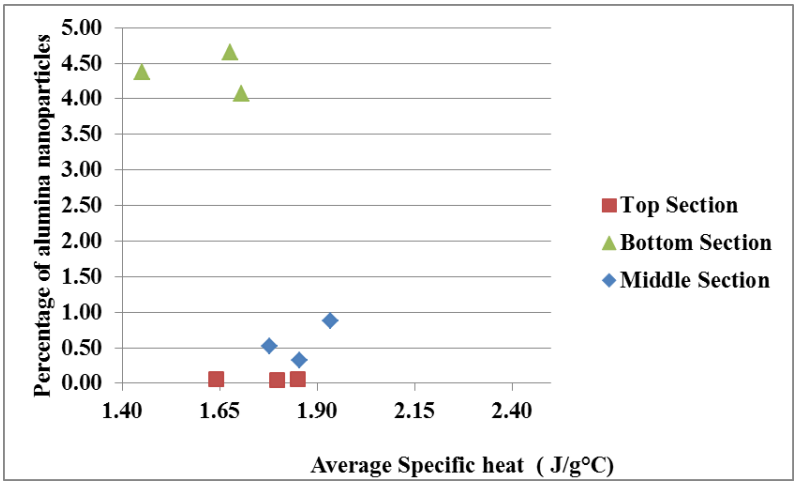

Graph correlating the concentration of nanoparticles with the specific heat in Batch A (Sample 3).

Batch B – (20 thermal cycles) Sample 4

		Specific heat J/g°C		
Section	**Specimen**	**Average of cycle 2 and cycle 3**	**Average of runs for each section**	**Std Deviation of runs for each section**
Top	1	2.0317	2.1003	0.0744
	2	2.1793		
	3	2.0899		
Middle	1	1.7865	1.8605	0.1330
	2	1.7810		
	3	2.0141		
Bottom	1	1.9156	1.8135	0.0994
	2	1.8076		
	3	1.7171		

Percentage of alumina			
Alumina %	Average %	Reported %	Smp STD
0.5132 0.4376 0.1111	0.3540	0.3401	0.2137
0.0107 0.0107 0.0160	0.0124	0.0113	0.0031
0.0364 0.0371 0.0135	0.0290	0.0302	0.0134

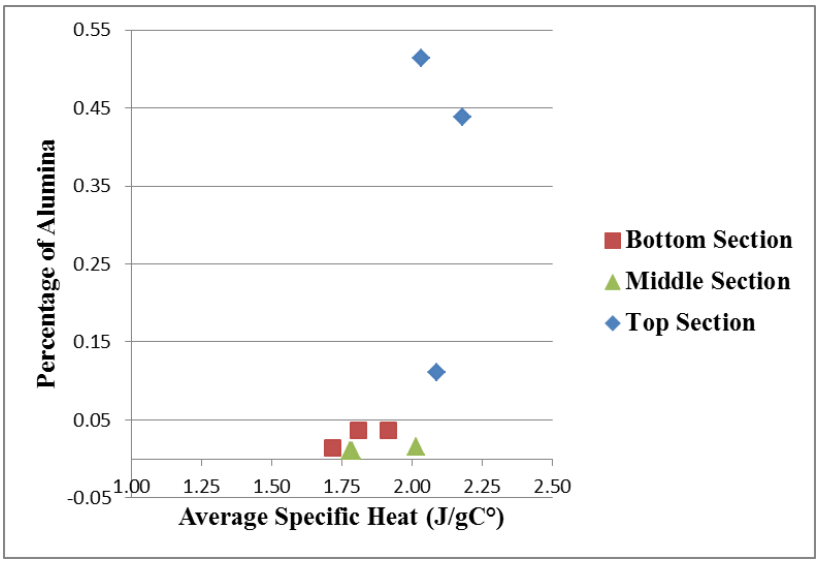

Graph correlating the concentration of nanoparticles with the specific heat in Batch B (Sample 4).

Batch B – (20 thermal cycles) Sample 5

		Specific heat J/g°C		
Section	**Specimen**	**Average of cycle 2 and cycle 3**	**Average of runs for each section**	**Std Deviation of runs for each section**
Top	1	2.2341	1.9768	0.3744
	2	2.1490		
	3	1.5472		
Middle	1	1.8201	1.7684	0.2473
	2	1.9858		
	3	1.4993		
Bottom	1	1.6709	1.7484	0.1198
	2	1.8865		
	3	1.6879		

Percentage of alumina			
Alumina %	**Average %**	**Reported %**	**Smp STD**
0.0346	0.0318	0.0302	0.0025
0.0310			
0.0298			
0.053	0.048	0.049	0.006
0.051			
0.041			
0.031	0.036	0.038	0.005
0.040			
0.036			

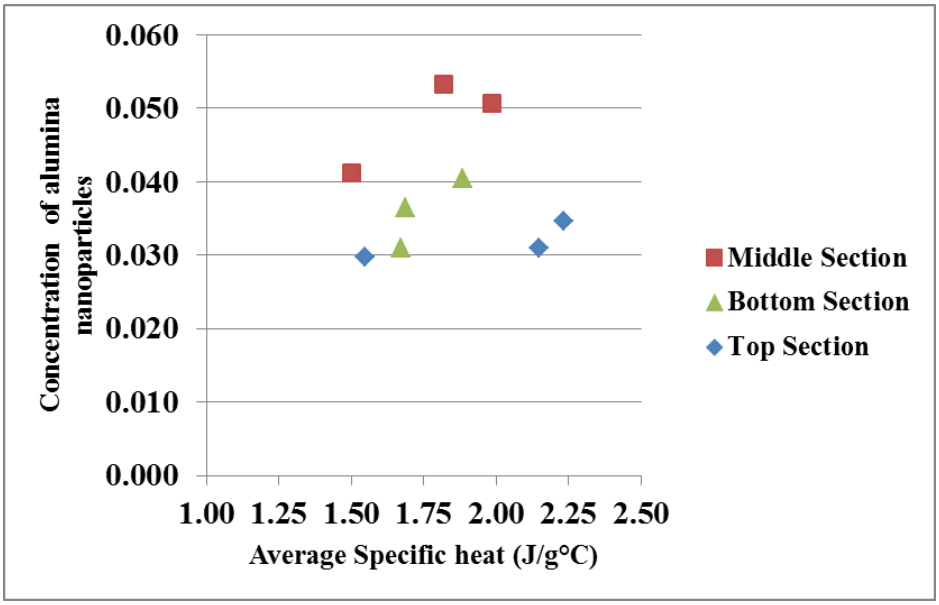

Graph correlating the concentration of nanoparticles with the specific heat in Batch B (Sample 5).

Batch B - 20 thermal cycles (Sample 6)

		Specific heat J/g°C		
Section	Specimen	Average of cycle 2 and cycle 3	Average of runs for each section	Std Deviation of runs for each section
Top	1	1.9530	1.9218	0.1325
	2	2.0359		
	3	1.7765		
Middle	1	1.9506	1.9417	0.0313
	2	1.9070		
	3	1.9676		
Bottom	1	2.0688	1.8863	0.2312
	2	1.6264		
	3	1.9639		

Percentage of alumina			
Alumina %	Average %	Reported %	Smp STD
0.0427 0.0469 0.0419	0.0438	0.0453	0.0026
0.035 0.062 0.044	0.047	0.045	0.014
0.043 0.045 0.041	0.043	0.042	0.002

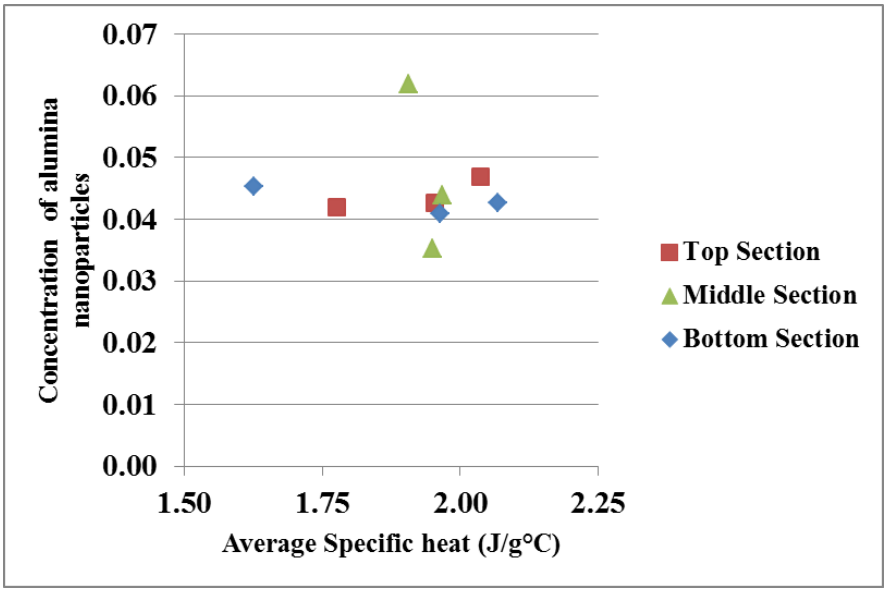

Graph correlating the concentration of nanoparticles with the specific heat in Batch B (Sample 6).

Batch C - 40 thermal cycles (Sample 7)

		Specific heat J/g°C		
Section	**Specimen**	**Average of cycle 1 and cycle 2**	**Average of runs for each section**	**Std Deviation of runs for each section**
Top	1	2.3966	2.2483	0.1418
	2	2.2345		
	3	2.1140		
Middle	1	2.0944	1.7743	0.3127
	2	1.4695		
	3	1.7592		
Bottom	1	2.0916	1.9253	0.1523
	2	1.9696		
	3	1.7148		

Percentage of alumina			
Alumina %	**Average %**	**Reported %**	**Smp STD**
0.0194	0.0230	0.0231	0.0049
0.0211			
0.0286			
0.0075	0.0099	0.0098	0.0021
0.0113			
0.0110			
1.4047	1.1210	1.1337	0.2553
1.0487			
0.9096			

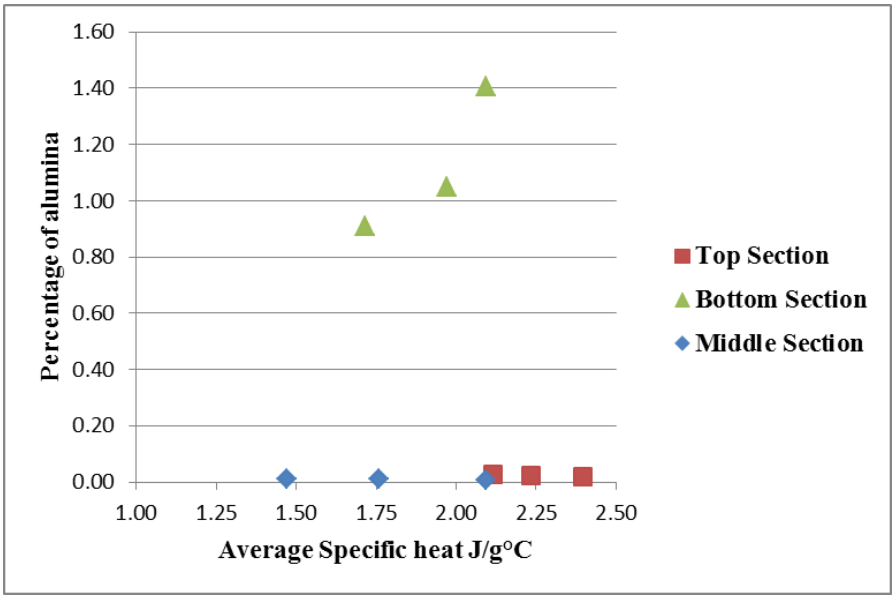

Graph correlating the concentration of nanoparticles with the specific heat in Batch C (Sample 7).

Batch C - 40 thermal cycles (Sample 8)

		Specific heat J/g°C		
Section	Specimen	Average of cycle 2 and cycle 3	Average of runs for each section	Std Deviation of runs for each section
Top	1	1.9262	1.9277	0.1146
	2	1.8139		
	3	2.0431		
Middle	1	1.5976	1.7063	0.1109
	2	1.8193		
	3	1.7019		
Bottom	1	1.8536	1.8459	0.1129
	2	1.7294		
	3	1.9548		

Percentage of alumina			
Alumina %	Average %	Reported %	Smp STD
0.0919 0.0449 0.0462	0.0610	0.0605	0.0268
0.0281 0.0192 0.0169	0.0214	0.0215	0.0059
0.3499 0.3524 0.5748	0.4257	0.4157	0.1291

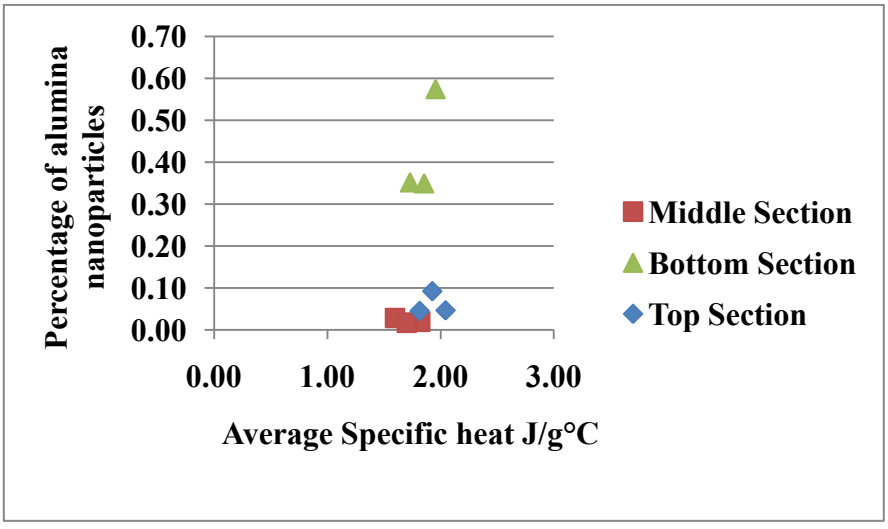

Graph correlating the concentration of nanoparticles with the specific heat in Batch C (Sample 8).

Batch C - 40 thermal cycles (Sample 9)

		Specific heat J/g°C		
Section	**Specimen**	**Average of cycle 2 and cycle 3**	**Average of runs for each section**	**Std Deviation of runs for each section**
Top	1	1.9629	1.9863	0.0874
	2	1.9130		
	3	2.0831		
Middle	1	1.8969	1.8923	0.0612
	2	1.9510		
	3	1.8289		
Bottom	1	1.9700	2.0271	0.0898
	2	1.9806		
	3	2.1306		

Percentage of alumina			
Alumina %	**Average %**	**Reported %**	**Smp STD**
0.0490	0.0561	0.0567	0.0352
0.0943			
0.0250			
0.0292	0.0326	0.0325	0.0031
0.0355			
0.0331			
0.0303	0.0327	0.0329	0.0021
0.0336			
0.0342			

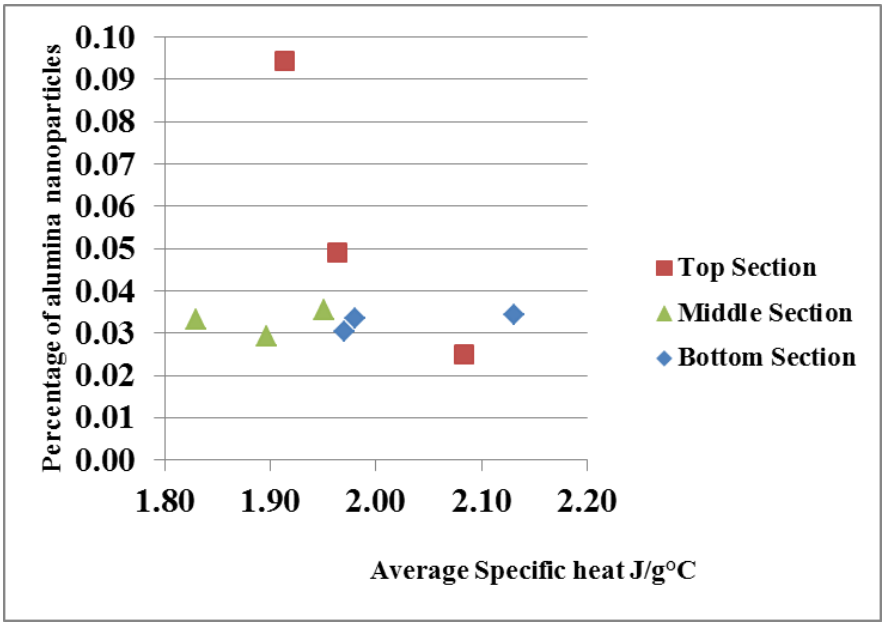

Graph correlating the concentration of nanoparticles with the specific heat in Batch C (Sample 9).

Batch D - 60 thermal cycles (Sample 10)

Batch D		Sample 10		
		Specific heat J/g°C		
Section	Specimen	Average of cycle 2 and cycle 3	Average of runs for each section	Std Deviation of runs for each section
Top	1	2.1348	1.9971	0.1573
	2	1.8257		
	3	2.0309		
Middle	1	2.0175	1.8836	0.1308
	2	1.7561		
	3	1.8773		
Bottom	1	1.6243	1.6658	0.0596
	2	1.6390		
	3	1.7341		

Percentage of alumina			
Alumina %	Average %	Reported %	Smp STD
0.018 0.011 0.026	0.019	0.019	0.007
0.034 0.031 0.030	0.032	0.032	0.002
0.055 0.050 0.048	0.051	0.051	0.003

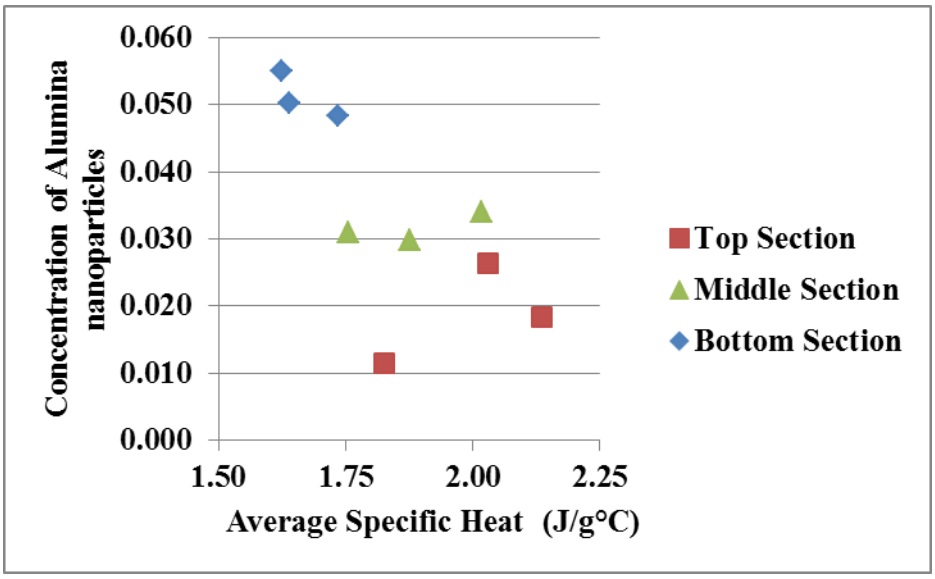

Graph correlating the concentration of nanoparticles with the specific heat in Batch D (Sample 10).

Batch D - 60 thermal cycles (Sample 11)

Batch D		Sample 11		
		Specific heat J/g°C		
Section	Specimen	Average of cycle 2 and cycle 3	Average of runs for each section	Std Deviation of runs for each section
Top	1	1.8528	1.8591	0.0144
	2	1.8756		
	3	1.8489		
Middle	1	1.7235	1.7104	0.0629
	2	1.7656		
	3	1.6420		
Bottom	1	1.8570	1.9024	0.0446
	2	1.9462		
	3	1.9039		

Percentage of alumina			
Alumina %	Average %	Reported %	Smp STD
0.014	0.019	0.019	0.005
0.023			
0.020			
0.009	0.008	0.008	0.002
0.006			
0.009			
0.016	0.105	0.106	0.086
0.187			
0.113			

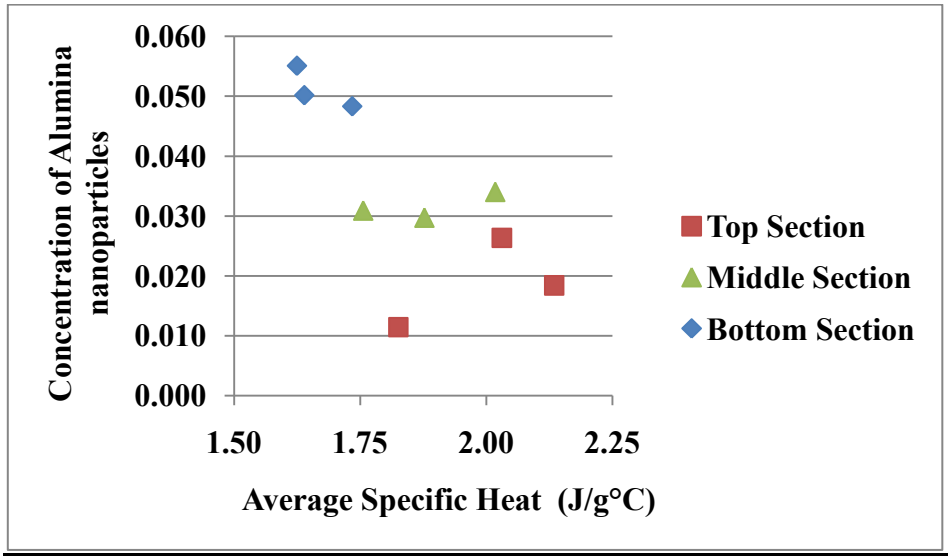

Graph correlating the concentration of nanoparticles with the specific heat in Batch D (Sample 11).

Batch D - 60 thermal cycles (Sample 12)

		Specific heat J/g°C		
Section	Specimen	Average of cycle 2 and cycle 3	Average of runs for each section	Std Deviation of runs for each section
Top	1	1.8154	1.7963	0.0515
	2	1.7381		
	3	1.8356		
Middle	1	1.7474	1.5840	0.2574
	2	1.2873		
	3	1.7172		
Bottom	1	1.8405	1.8710	0.0591
	2	1.8334		
	3	1.9392		

Percentage of alumina			
Alumina %	Average %	Reported %	Smp STD
0.028 0.029 0.080	0.046	0.045	0.030
0.034 0.032 0.028	0.031	0.031	0.003
0.197 0.124 0.094	0.138	0.140	0.053

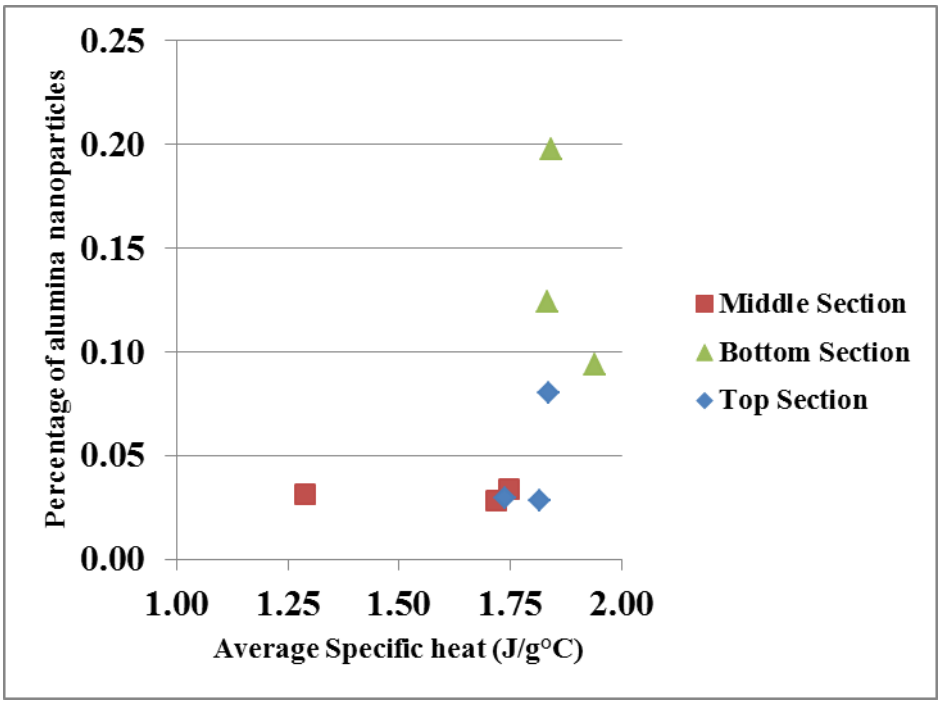

Graph correlating the concentration of nanoparticles with the specific heat in Batch D (Sample 12).

APPENDIX C

HEAT TRANSFER CALCULATIONS FOR THE MATERIAL IN THE CENTRE OF THE CYLINDER

The thermal profile used for carrying out the thermal cycling test was designed by keeping in mind the time the required for the entire material to be uniformly heated. The Figure 19 shows the cross sectional view of the cylinder containing the sample material

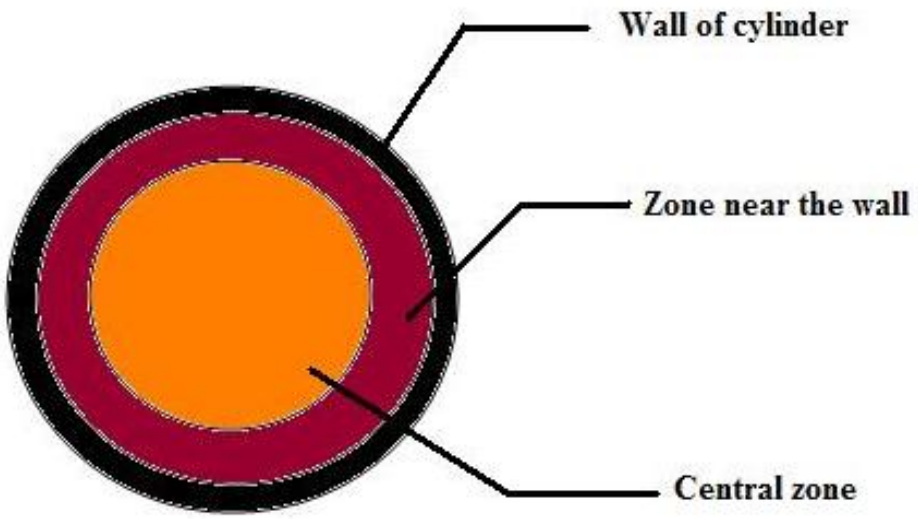

Figure 19 : Cross sectional view of the sample tube

The cross sectional view of the sample tube shows that there are 3 different zones. The first is the wall of the sample tube which is made of stainless steel (SS 316 grade).The second is a thin layer of material near the wall. The third is the bulk of the material which is the material in the central portion of the sample tube. Through heat transfer calculations it has to be shown that the temperature of central portion of the sample tube is the same as the temperature of the material near the wall. A significant difference in the temperature between the material near the wall and the material in the central will result in confounding the experiment. Using one dimensional

transient heat transfer calculations and Heisler's chart it is shown that the difference between the temperature of material in the centerline of the sample tube and the temperature of the wall of the sample tube is very small.

One dimensional Transient heat transfer

The ratio θ can be obtained from Heisler's chart.

$\theta = (T_o - T_\infty)/(T_i - T_\infty)$

where

T_o = Temperature of the material in the central zone of the tube after time't'

T_i = Initial temperature of the material.

T_∞ = Temperature of the air surrounding the sample tube.

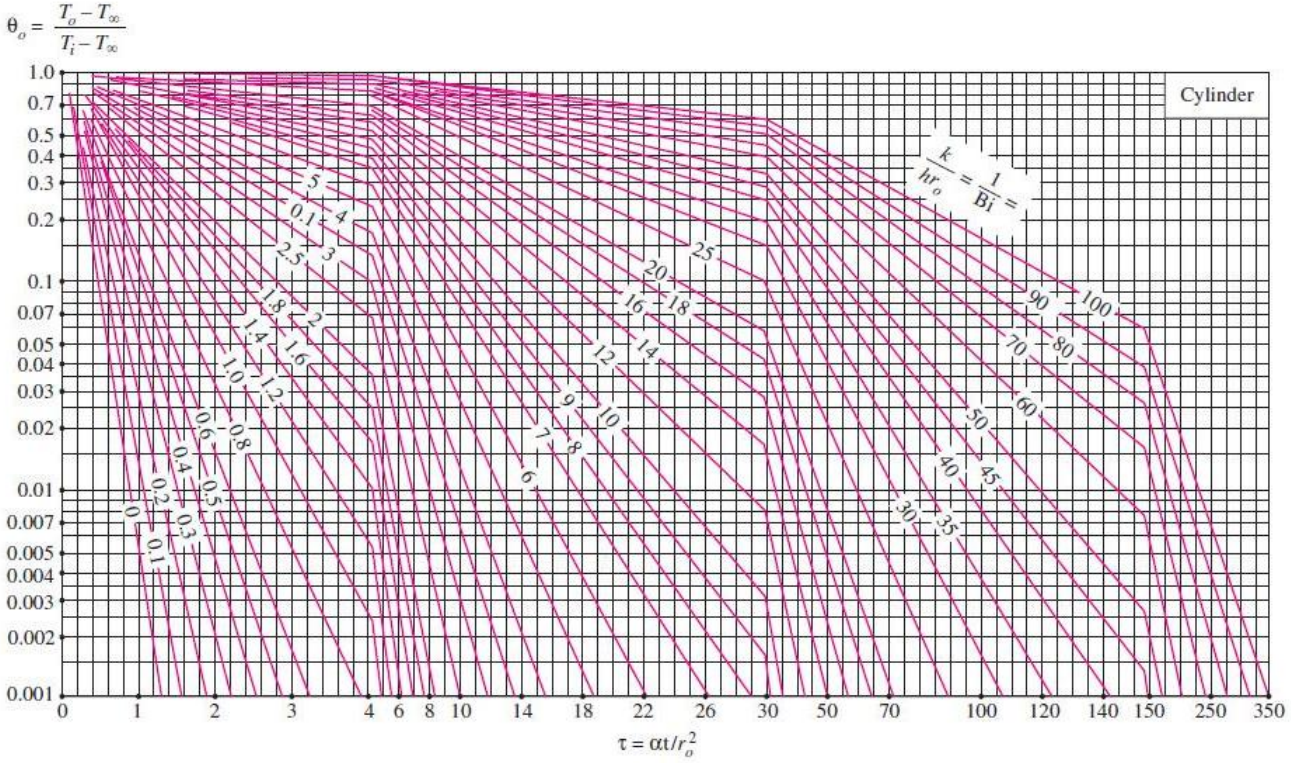

Figure 20 : Heisler's chart showing centerline temperature in a cylinder (22)

Using the Heisler's chart from Figure 20 the temperature of the material in the centerline can be calculated.

The other non dimensional parameter calculation is shown.

i) $\tau = \alpha t / r_o^2$

α = thermal diffusivity of the material = $2.002*10^{-7}$ m^2s^{-1}

t = time , second

r_o = radius of the cylinder = 0.00476 m

ii) $1/Bi = k/hr_o$

k = thermal conductivity of the material = 0.6265 $Wm^{-1}K^{-1}$

h = heat transfer coefficient of the air surrounding the cylinder = 10 $Wm^{-2}K^{-1}$

The values of thermal diffusivity and thermal conductivity of the base material as available in literature (9) have been used for this calculation.

When time is equal to 30 minutes the value of θ obtained from the chart is equal to 0.09.The value of θ keeps decreasing with increase in time .A time interval of 1 hour further reduces the value of θ to 0.007.A small value of θ indicates that the centerline of the sample tube is closer to the temperature of the medium surrounding the sample tube.

The medium surrounding the sample tube in our case is the air inside the furnace. Air temperature measured inside the furnace show that the temperature measured by the thermocouple of the furnace agrees with the temperature of air inside the furnace.

With a small value of θ indicates that the time period of 1 hour is sufficient for the material present in the centerline of the sample tube to reach the design temperature in the thermal profile.

VITA

Name: Sandhya Shankar

Address: C/O Dr.Sai Lau

Department of Mechanical Engineering

Texas A&M University

College Station,Texas -77843-3123

Email Address: s.sandhya11@neo.tamu.edu

Education: M.S.,Texas A&M University,May 2011

B.E.,College of Engineering,Guindy,Anna University,June 2007